EFFICIENT LOW-SPEED FLIGHT IN A WIND FIELD

by

Michael A. Feldman

Thesis submitted to the Faculty of the
Virginia Polytechnic Institute and State University
in partial fulfillment of the requirements for the degree of

MASTER OF SCIENCE IN AEROSPACE ENGINEERING

APPROVED:
Eugene M. Cliff, Chair
Frederick H. Lutze
Wayne C. Durham

July 24, 1996
Blacksburg, Virginia

Keywords: Optimization, Optimal Control, Aircraft Performance

EFFICIENT LOW-SPEED FLIGHT IN A WIND FIELD

Michael A. Feldman

(ABSTRACT)

A new software tool was needed for flight planning of a high altitude, low speed unmanned aerial vehicle which would be flying in winds close to the actual airspeed of the vehicle. An energy modeled NLP formulation was used to obtain results for a variety of missions and wind profiles. The energy constraint derived included terms due to the wind field and the performance index was a weighted combination of the amount of fuel used and the final time. With no emphasis on time and with no winds the vehicle was found to fly at maximum lift to drag velocity, V_{md}. When flying in tail winds the velocity was less than V_{md}, while flying in head winds the velocity was higher than V_{md}. A family of solutions was found with varying times of flight and varying fuel amounts consumed which will aid the operator in choosing a flight plan depending on a desired landing time. At certain parts of the flight, the turning terms in the energy constraint equation were found to be significant. An analysis of a simpler vertical plane cruise optimal control problem was used to explain some of the characteristics of the vertical plane NLP results.

Acknowledgment

I am grateful to Dr. Eugene Cliff for the help and guidance he has given me. I also wish to thank Dr. committee.

Contents

List of Figures

Nomenclature

x, y	Horizontal position coordinates
h	Altitude
V	Vehicle velocity with respect to surrounding air
γ	Flight path angle with respect to surrounding air
χ	Heading angle with respect to surrounding air
μ	Bank angle
W_f	Weight of fuel consumed
t	Time
V_w	Wind velocity
χ_w	Wind heading angle
V_I	Inertial velocity
T	Thrust
D	Drag
L	Lift
m	Mass
g	Acceleration due to gravity
n	Load factor
c	Power specific fuel consumption
P_a	Power available
P_r	Power required
P_s	Specific excess power
ξ	Throttle setting
η	Propeller efficiency
R	Range
W	Aircraft weight
W_s	Standard weight
W_t	Test or current weight
ρ	Air density
ρ_o	Air density at standard sea level
σ	Ratio of air density to sea level air density
S	Wing surface area
C_L	Lift coefficient
C_D	Drag coefficient
C_{D_o}	Parasite drag coefficient
E	Absolute energy
H	Variational Hamiltonian
N_p	Number of waypoints

Chapter 1

Introduction

Problems associated with finding the 'best' path for an object have long been of interest to both mathematicians and practitioners. The classical brachistochrone problem, proposed by John Bernoulli in 1696 [1] is an example of an early problem that led to the development of the Calculus of Variations. In more recent times, the problem of optimal ascent of a rocket-powered vehicle proposed by Robert Goddard (see [2] for example), provided motivation for modern development in trajectory optimization.

As noted optimal shaping of aerospace trajectories has provided the motivation for much recent study of modern optimization theory and algorithms. Current industrial practice favors approaches where the continuous-time optimal control problem is transcribed to a finite-dimensional Non-Linear Programming problem (NLP) by a discretization process. Two such general formulations are implemented in the POST [3] and the OTIS [4] codes.

There are several existing codes for various flight planning applications. The OPTIM [5] code, developed by Analytical Mechanics Associates, Inc., and the MITRE [6] code were written to be used for flight planning purposes or as part of an on-board flight management system for general aviation or turbojet transport aircraft. Both codes minimize fuel consumption or direct operating costs. Only the vertical plane aspects of the flight are optimized in these codes. The horizontal position coordinates that the vehicle follows are predetermined depending on the locations of navigational aids and airports.

1.1 Flight Problem

The motivation for this work is flight-planning for the Theseus vehicle, built by Aurora Flight Sciences. The aircraft is to be used to sample the atmosphere over the South Pole and is to operate for the most part in an autonomous fashion. The aircraft data specific to Theseus are included in Appendix C. While the numerical results are specific to the Theseus airplane, the approach is rather general and applies to similar vehicles which fly at low speeds in wind fields. The nominal mission includes take-off, long-range flight to

a remote site of interest near the South Pole, a scientific data-collection leg and return to base. A ground-based human pilot will perform take off and landing but the aircraft acts like a robot during the remainder of its flight. It is controlled by providing specific coordinates or waypoints to fly through and by providing speed and altitude commands. This waypoint idea will be discussed further in Chapter 3.

The science mission requires flight over a prescribed path at a prescribed altitude. We are not focusing on trajectory shaping for this part of the flight since it is mostly defined by the scientific data requirements. The vehicle is to operate at high altitudes (60,000 - 80,000 feet) during this science leg of the mission. The vehicle will fly from Christchurch, New Zealand to the vicinity of the South Pole, take data, and fly back. It is about 2800 nautical miles from the base to the Pole. The wind-field is presumed known (and persistent); its magnitude is expected to be a significant fraction of the vehicle's true airspeed. Average winds at these altitudes are substantial as will be seen by a figure in Chapter 5. A wind model obtained from NASA Goddard Space Flight Center describes horizontal winds which are in a clockwise direction around the Pole. The wind speed depends on the distance from the pole and on the altitude.

The specific problem for flight planning is getting back to the base. Given the winds and the current 'state' of the vehicle can it return safely? Since the vehicle is landed by a human operator it is preferable to land during daylight hours. In addition, since the vehicle is flimsy due to its low wing loading, we do not want to land in bad weather. Thus, we are interested in the range of possible times when we can get back. Will there be sufficient light? Will the local weather be okay? To answer these questions we pose a family of flight optimization problems where the performance index is a weighted combination of fuel and time (i.e. $J = W_f + \mu\ t_f, \mu \geq 0$). The weighting parameter μ defines a one-parameter family of flight optimization problems. There should be a family of solutions of varying times to return home and fuel consumed. The limits will correspond to the longest time to return home which will also be the most fuel efficient path and the shortest time to return home.

In the present paper a discretization is used that is specially adapted to the flight problem of interest. Among the unique aspects of the present discretization are: a least-squares formulation for certain kinematic constraints; the use of energy ideas to enforce Newton's Laws; and, the inclusion of large magnitude horizontal winds. In order to offer more flexibility in the presence of the strong horizontal winds, the horizontal path is not fixed as it was in the OPTIM and MITRE codes. Energy exchange due to turning will also be included.

2

1.2   Overview

In order to solve the flight planning problem a mathematical model is necessary. Various levels of fidelity are available such as point-mass, energy, and cruise modeling. In the next chapter a description of the various models available and reasons to use each one are provided. Following this is the development of the finite dimensional energy model. This development includes the derivations of the constraint equations to use in the computer code to solve the problem. Chapters 4 and 5 discuss some results from running vertical plane and full three dimensional versions of the energy model code. Chapter 6 explains some of the results using a simple, vertical-plane, continuous optimal control problem.

Chapter 2

Modeling

An appropriate mathematical model is needed in solving the current flight planning problem. In stability and control a highly detailed mathematical model including rigid body mechanics is usually used. However, this is a flight performance problem so only motion of the vehicle as a whole is of interest. Positions and motions of the control surfaces on the vehicle, for example, are not important in this type of problem so the most detailed model needed in flight performance is a point mass model. Simplified, reduced order versions of the point mass model are also available and these include the energy model and the cruise model.

2.1   Point Mass Model

The derivation of the point mass model for symmetric flight over a flat, non-rotating Earth with horizontal winds is in Appendix A. While the point-mass model is high fidelity, it is not best for our purposes. The reason is that in the point-mass model the controls are directly related to forces - small disturbance motions include the phugoid mode and four zero eigenvalues (3 corresponding to position and one to heading). Thus the system has 4 poles at the origin and is very difficult to control. Many waypoints close together would be needed to capture the dynamics of the phugoid oscillations for example. A more approximate model with less dynamics is necessary in this case. Here we focus on the energy model first developed by Kaiser [7].

2.2   Energy Model

In this model velocity and altitude are combined into a single variable energy. The absolute energy is defined to be the sum of the potential and kinetic energy per unit weight. The term *absolute* is to remind us that the kinetic energy is computed from the inertial velocity, $\vec{V_I}$,

as defined in Appendix A. The differential equations for altitude and path angle evolution are equilibrated, reducing the dynamic order of the model. In the vertical plane case five state variables (two position, two velocity and weight) are reduced to three state variables (range, energy and weight). An energy constraint equation ensures that the change in total energy from one point to another is equal to the work done by the net external force acting on the vehicle. This model is simpler than the point-mass model and is the one which will be used to develop the computer code.

2.3   Cruise Model

To get a cruise model the energy model is simplified even more by equilibrating the energy state. This leaves only two state variables (range and fuel weight consumed). This model will be used for an analysis of the continuous optimal control problem to characterize the nature of optimal paths in Chapter 6.

Chapter 3

Finite Dimensional Energy Model

In keeping with modern practice [3, 4] we shall approximate the flight problem by a finite-dimensional transcription. Rather than considering the state/control variables as 'arbitrary' functions of time, we shall prescribe their values at certain points, along with appropriate rules for interpolating between these points (in our case a mixture of piecewise linear and piecewise constant approximation). This approach has the effect of replacing the infinite-dimensional problem (find the state/control functions) with a finite-dimensional problem (find certain state/control values). Since the models are generally nonlinear we have a Non-Linear Programming problem (NLP).

Our goal is to develop an efficient NLP formulation for the flight planning problem, including the important effects of winds. The NLP framework requires that we identify a parameterization of the flight path, a scalar-valued cost functional and vector-valued constraints. The constraint functions must enforce the important physics of the flight problem to a reasonable level of approximation.

It is convenient to parameterize the set of possible flight paths in terms of quantities that are useful in the flight guidance problem. As noted previously, the guidance of the vehicle is naturally implemented in terms of *waypoints*. Certain waypoints through which the airplane will fly are specified. Figure 3.1 illustrates a horizontal projection of four such waypoints. At each waypoint we consider the following variables:

- x, y, h horizontal position coordinates and altitude

- V, χ speed and heading, relative to the air mass

- E total mechanical energy per unit weight

- m remaining mass
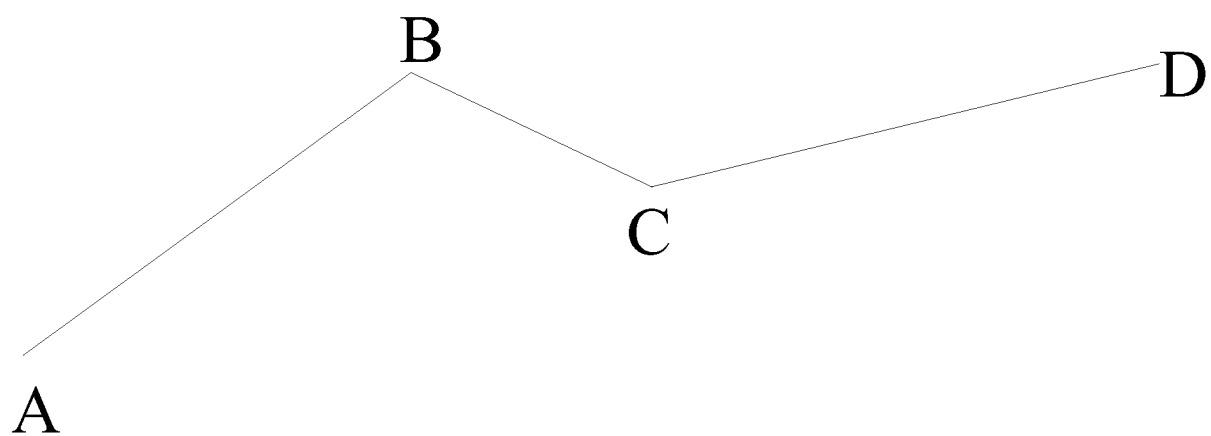
- ξ throttle setting

Figure 3.1: Projection of Waypoints in the Horizontal Plane

For conceptual purposes we consider a point-mass model wherein the dynamics are described by Newton's Laws. The 'states' and 'controls' will be recorded at each waypoint. The variables include position coordinates, velocity with respect to the surrounding air mass, heading angle and vehicle mass. All of these variables, except heading angle, are imagined to change smoothly between waypoints. The heading angle will be assumed to be nearly constant between waypoints; any change will occur in a short period of time in the vicinity of each waypoint. For concreteness it is imagined that this heading change occurs as we approach a waypoint. For the bulk of the flight from waypoint i to point $i + 1$ the relative velocity heading angle is constant at the value χ_i. Controls include the throttle setting, ξ, and are taken to be piecewise constant from a 'departing' waypoint to the next ('arriving') waypoint and then to change instantly at the 'arriving' waypoint. The wind velocity is a smooth function of position.

We envision that the waypoints are well separated so that the flight path inclination (γ) is small. Vertical equilibrium of the aircraft will require equality of lift and weight. Additionally, along this path the net work done on the vehicle must equal the change in kinetic energy. Finally, the weight change must balance the integral of the fuel rate. A detailed description of the various constraints is now presented.

3.1   Horizontal Path Constraint

Here the requirement that the integrated path segment must connect adjacent waypoints is enforced. For notational convenience, let $\vec{r}$ represent the horizontal position components; and, let $\vec{v}$ represent the horizontal plane projection of the vehicle's velocity (relative to the air mass). $\vec{V}_w$ is the wind-field which has been assumed horizontal.

We have

$$\dot{\vec{r}} = \vec{v} + \vec{V}_w \quad \text{or} \quad \vec{r}_{i+1} - \vec{r}_i - \int_{t_i}^{t_{i+1}} \left[\vec{v}(t) + \vec{V}_w(\vec{r}(t), h(t)) \right] dt = 0 \tag{3.1}$$

The integral in (3.1) is approximated by averaging the integrand over the flight segment. For the moment we defer a detailed description of this averaging and simply introduce the symbol $\vec{v}_i^A$ for its value.

The constraint (3.1) is written as:

$$\vec{e}_i = \vec{r}_{i+1} - \vec{r}_i - \vec{v}_i^A (t_{i+1} - t_i) = 0$$

The vector quantities may be computed from the data at the waypoints. Note, however, that we have elected not to include time in our parameter list. Instead, we solve for $\Delta t_i \equiv (t_{i+1} - t_i)$ from the least-squares problem

$$\min_{\Delta t} \|\vec{e}_i\|^2.$$

8

This leads to the requirement

$$\left\langle (\vec{r}_{i+1} - \vec{r}_i) - \vec{v}_i^A \Delta t_i \, , \vec{v}_i^A \right\rangle = 0 \quad \Rightarrow \quad \Delta t_i = \frac{\left\langle (\vec{r}_{i+1} - \vec{r}_i) \, , \vec{v}_i^A \right\rangle}{\|\vec{v}_i^A\|^2}. \tag{3.2}$$

With this Δt_i in hand, one can compute the norm of the residual error from

$$\|\vec{e}_i\|^2 = \|\Delta \vec{r}_i\|^2 - \|\vec{v}_i^A \Delta t_i\|^2$$

where $\Delta \vec{r}_i = \vec{r}_{i+1} - \vec{r}_i$. It is tempting to impose the constraint $\|\vec{e}_i\|^2 = 0$. Unfortunately, since this constraint is quadratic, we find that when the constraint vanishes, so does its gradient. This will introduce a loss-of-rank feature in the Kuhn-Tucker optimality system at the solution point and cause considerable trouble in the NLP problem (see [8], p 78 *ff*). Instead we opt for a different pathology and impose the scalar constraint that the y component of the residual $\vec{e}_i$ vanish. This leads to

$$(y_{i+1} - y_i) \|\vec{v}_i^A\|^2 - v_{i\,y}^A \left\langle \Delta \vec{r}_i, \ \vec{v}_i^A \right\rangle = 0 \tag{3.3}$$

The choice of y component over x component is arbitrary. Note that for some geometries the constraint (3.3) may be satisfied while the path is not kinematically feasible. We must test any numerical 'solution' of our problem to ensure this situation does not occur. We will also include an inequality constraint

$$\Delta t_i - \Delta t_{\min} \geq 0 \tag{3.4}$$

where $\Delta t_{\min}$ is some prescribed minimum allowable time. The constraint (3.4) ensures that time goes forward and, loosely, that the waypoints are not 'too close'.

3.1.1 Calculation of $\vec{v}_i^A$

We use an implicit Euler rule and calculate the integrand as the simple average of 'left' and 'right' values. That is, we have

$$\vec{v}_i^A = (1/2) \left(\vec{v}_i^L + \vec{v}_i^R \right),$$

with

$$\begin{aligned}
\vec{v}_i^L &\equiv \vec{V}_w(\vec{r}_i) + V_i \left(\cos \chi_i \ \hat{e}_x \ + \ \sin \chi_i \ \hat{e}_y \right) \\
\vec{v}_i^R &\equiv \vec{V}_w(\vec{r}_{i+1}) + V_{i+1} \left(\cos \chi_i \ \hat{e}_x \ + \ \sin \chi_i \ \hat{e}_y \right).
\end{aligned}$$

Note that we have used the heading χ_i in both the $\vec{v}_i^L$ and the $\vec{v}_i^R$ expressions, whereas the remaining data are local to the waypoint. Our model supposes that the changes in local airspeed and wind-field are smooth, whereas the heading change is concentrated as we 'arrive' at the waypoint. For all but the last few seconds of this flight segment we have $\chi(t) = \chi_i$.

3.2 Energy Change Constraint

We start with Newton's Second Law.

$$m\dot{\vec{V}}_I = \vec{F} \tag{3.5}$$

where $\vec{V}_I$ is the inertial velocity:

$$\vec{V}_I = \vec{V} + \vec{V}_w \tag{3.6}$$

Distance traveled is expressed by equation (3.6) multiplied by the change in time. The force in equation (3.5) is dotted with this distance to get an expression for energy.

$$m\dot{\vec{V}}_I \cdot \vec{V}_I \, dt = \vec{F} \cdot (\vec{V} + \vec{V}_w) \, dt \tag{3.7}$$

To continue with the derivation of the energy constraint equation two special cases will be considered separately: wings level flight and turning flight. Each of these conditions will affect the force in equation (3.7) differently.

3.2.1 Wings-Level Flight

We now analyze the wings-level flight segment between adjacent waypoints. Note this is the bulk of the flight since the turning is supposed to happen in the brief time preceding arrival at the new waypoint. Expanding the force in equation (3.5) yields the following equation.

$$\vec{F} = (T - D) \, \hat{e}_t + L \, \hat{e}_n + mg \, \hat{e}_z \tag{3.8}$$

where

$\hat{e}_t$ is a unit vector tangential to $\vec{V}$,
$\hat{e}_n$ is a unit vector normal to $\vec{V}$ in the vertical plane,
$\hat{e}_z$ is a unit vector in the direction of gravity.

These unit vectors are illustrated in Figure 3.2. The drag, D, in equation (3.8) is the level flight drag with a load factor of $n = 1$. Substituting equation (3.8) into equation (3.7):

$$m\dot{\vec{V}}_I \cdot \vec{V}_I \, dt = [(T - D)\hat{e}_t + L\hat{e}_n] \cdot \vec{V} dt + [(T - D)\hat{e}_t + L\hat{e}_n] \cdot \vec{V}_w dt + mg\hat{e}_z \cdot (\vec{V} + \vec{V}_w) \, dt \tag{3.9}$$

Since $\vec{V} = V\hat{e}_t$, equation (3.9) is simplified slightly.

$$m\dot{\vec{V}}_I \cdot \vec{V}_I \, dt = (T - D) \, V \, dt + [(T - D)\hat{e}_t + L\hat{e}_n] \cdot \vec{V}_w dt + mg\hat{e}_z \cdot (\vec{V} + \vec{V}_w) \, dt \tag{3.10}$$

The absolute specific energy is defined to be the sum of the potential and kinetic energy per unit weight.

$$E \equiv \frac{1}{2g}(\vec{V}_I \cdot \vec{V}_I) + h \tag{3.11}$$

10
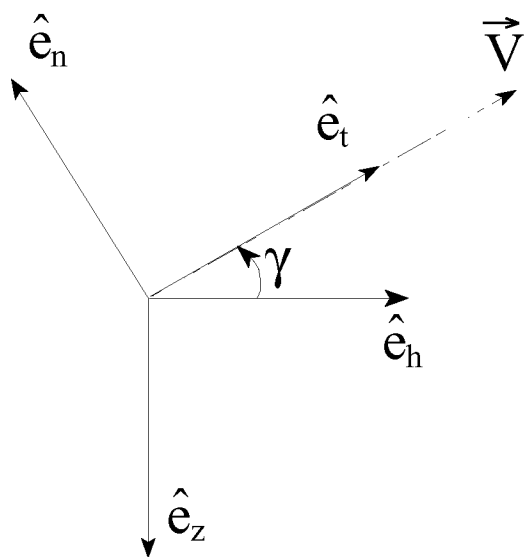
Vertical Plane
Projection
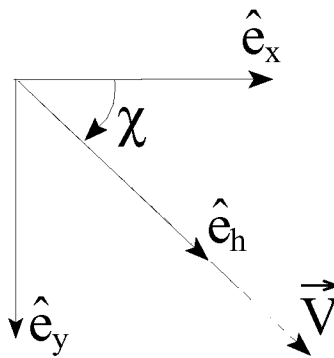
Horizontal Plane
Projection

Figure 3.2: Unit Vectors

11

Taking the derivative with respect to time, the following is obtained:

$$\frac{dE}{dt} = \frac{1}{g}(\dot{\vec{V_I}} \cdot \vec{V_I}) + \dot{h}$$

After substituting $\dot{h} = -(\vec{V} + \vec{V_w}) \cdot \hat{e}_z$ and multiplying both sides by the differential dt we get

$$dE = \frac{1}{g}(\dot{\vec{V_I}} \cdot \vec{V_I}) \, dt - (\vec{V} + \vec{V_w}) \cdot \hat{e}_z \, dt \qquad (3.12)$$

Combining equations (3.10) and (3.12) with simple manipulations leads to:

$$dE = \left(\frac{T-D}{mg}\right) V \, dt + \left[\frac{T-D}{mg}\hat{e}_t + \frac{L}{mg}\hat{e}_n\right] \cdot \vec{V_w} dt$$

This form is integrated to yield

$$\int dE = \int \frac{(T-D)}{mg} V \, dt + \int \left[\frac{T-D}{mg}\hat{e}_t + \frac{L}{mg}\,\hat{e}_n\right] \cdot \vec{V_w} \, dt \qquad (3.13)$$

The integrand of the first term on the right side of equation (3.13) is the specific excess power, $P_s \equiv (T-D)V/mg$. The product $T\,V$ is the *power available*, P_a, while the product $D\,V$ is the *power required*, P_r. The other two terms in equation (3.13) are given temporary names so they can be evaluated separately.

$$\begin{aligned}
T_1 &\equiv \left(\frac{T-D}{mg}\right)\hat{e}_t \cdot \vec{V_w} \\
T_2 &\equiv \left(\frac{L}{mg}\right)\hat{e}_n \cdot \vec{V_w},
\end{aligned} \qquad (3.14)$$

Equation (3.13) becomes

$$\int dE = \int P_s \, dt + \int [T_1 + T_2] \, dt$$

From Figure 3.2 we see that the tangent vector can be represented as

$$\hat{e}_t = \cos\gamma \, \hat{e}_h - \sin\gamma \, \hat{e}_z$$

where $\hat{e}_h$ is a unit vector in the direction of the horizontal projection of the aircraft velocity. T_1 now becomes

$$T_1 = \left(\frac{T-D}{mg}\right)\left[\cos\gamma \, (\hat{e}_h \cdot \vec{V_w}) - \sin\gamma \, (\hat{e}_z \cdot \vec{V_w})\right] \qquad (3.15)$$

However, in our model the winds are in the horizontal direction only, so when the wind vector is dotted with $\hat{e}_z$, a vertical unit vector, the second term in the brackets disappears.

12

The horizontal unit vector, $\hat{e}_h$, can be written as $\hat{e}_h = \cos \chi \; \hat{e}_x + \sin \chi \; \hat{e}_y$ and substituted into equation (3.15).

$$T_1 = \left(\frac{T - D}{mg} \right) \cos \gamma \; \cos(\chi_w - \chi) \; V_w$$

where χ_w is the heading angle of the wind velocity and $V_w \equiv \|\vec{V}_w\|$. T_1 is multiplied and divided by the aircraft velocity, V, to get an expression in terms of specific excess power which can be calculated.

$$T_1 = \left(\frac{P_s \, V_w}{V} \right) [\cos \gamma \; \cos(\chi_w - \chi)]$$

Now the T_2 term will be evaluated. Since the vehicle is assumed to be in symmetric flight, lift can be written as

$$L = mg \cos \gamma \tag{3.16}$$

The normal unit vector, $\hat{e}_n$, can be written as

$$\hat{e}_n = -\sin \gamma \; \hat{e}_h - \cos \gamma \; \hat{e}_z \tag{3.17}$$

Equations (3.16) and (3.17) are substituted into expression (3.14) to yield:

$$T_2 = -\cos \gamma [\sin \gamma (\hat{e}_h \cdot \vec{V}_w) + \cos \gamma (\hat{e}_z \cdot \vec{V}_w)]. \tag{3.18}$$

Again, because the winds are horizontal, equation (3.18) simplifies to

$$T_2 = -\cos \gamma \sin \gamma \cos(\chi_w - \chi) V_w.$$

This equation is multiplied and divided by the aircraft velocity, V, so that $V \sin \gamma$ can be written as the vertical velocity, $\dot{h}$, and T_2 becomes

$$T_2 = -\frac{V_w}{V} \cos \gamma \cos(\chi_w - \chi) \dot{h}$$

Using the assumption that the path angle (γ) is small and $\cos \gamma \approx 1$, T_1 and T_2 can be written as

$$T_1 = P_s \frac{V_w}{V} \cos(\chi_w - \chi) \tag{3.19}$$

$$T_2 = -\frac{V_w}{V} \cos(\chi_w - \chi) \dot{h} \tag{3.20}$$

We define a new variable, $\mathcal{F} \equiv \frac{V_w}{V} \cos(\chi_w - \chi)$. After substituting $\mathcal{F}$ into equations (3.19) and (3.20), T_1 and T_2 finally become

$$T_1 = \mathcal{F} \, P_s$$
$$T_2 = -\mathcal{F} \, \dot{h}$$

13

The absolute energy integral can now be written as

$$\int dE = \int P_s \, dt + \int P_s \, \mathcal{F} \, dt - \int \mathcal{F} \, dh \qquad (3.21)$$

Rearranging terms, the energy balance equation is

$$\int dE = \int P_s (1 + \mathcal{F}) \, dt - \int \mathcal{F} \, dh \qquad (3.22)$$

Note that for the case with no winds $\mathcal{F} = 0$ and equation (3.22) reduces to the usual energy integral result.

3.2.2   Turning Segment

There is also energy exchange in the turn in the vicinity of each waypoint. During the turn there will be a horizontal component of the lift vector denoted by $\|\vec{L_h}\| = L \sin \mu$, where μ is the vehicle bank angle. This force is dotted with the inertial velocity and integrated over time to get the work done in the turn.

$$\text{Work due to banked turn} = \int \vec{L_h} \cdot (\vec{V} + \vec{V_w}) dt$$

The force is perpendicular to the vehicle velocity, $\vec{L_h} \cdot \vec{V} = 0$, while the contribution from the wind velocity leads to

$$\text{Work due to banked turn} = \int L \sin \mu \, V_w \cos(\chi + \frac{\pi}{2} - \chi_w) \, dt. \qquad (3.23)$$

Instead of integrating over time it is more convenient to integrate over the change in heading angle. To produce this change of independent variable the third equation in (A.23) used. Assuming that the winds are constant near the waypoint and that the flight path angle, γ, is zero, we observe the familiar result:

$$mV\dot{\chi} = L \sin \mu$$

or in differential form:

$$L \sin \mu \, dt = mV d\chi \qquad (3.24)$$

Equation (3.24) is now substituted into equation (3.23) to get an equation which can be integrated over the heading angle.

$$\begin{aligned} \text{Work due to banked turn} \quad &= \quad \int mVV_w[-\sin(\chi - \chi_w)] \, d\chi \\ &= \quad mVV_w[\cos(\chi_w - \chi)]|_a^b. \end{aligned} \qquad (3.25)$$

One special case of this work in a banked turn would be similar to a problem presented in Halfman [9]. Suppose the airplane starts out flying directly against the wind at the

14

Horizontal Plane

L

μ

L sin μ

W

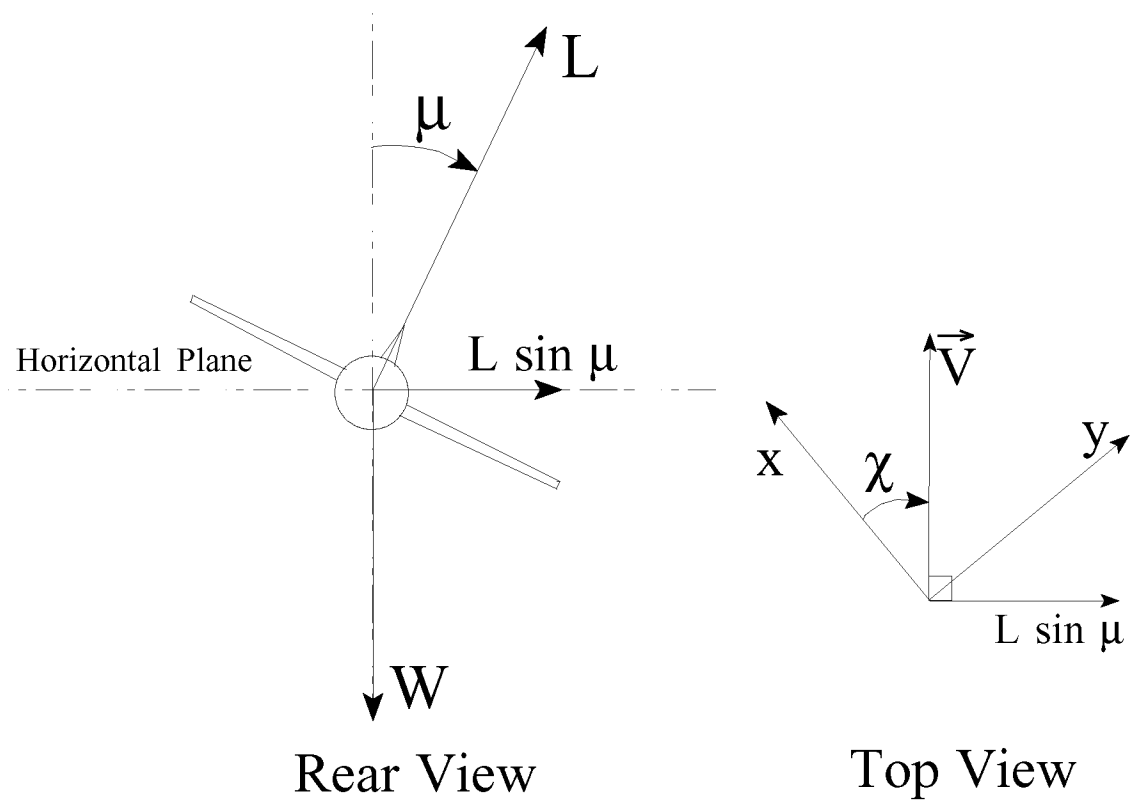Rear View

$\vec{V}$

x

χ

y

L sin μ

Top View

Figure 3.3: Front View of Airplane in Banked Turn

same velocity magnitude as the wind. After a 180° turn the plane would be flying in the same direction as the wind and at the same relative velocity magnitude. This means that $\chi(b) = \chi_w$, $\chi(a) = \chi_w - \pi$, $V = V_w$. Using equation (3.25) in this example, the work due to banked turn $= 2\,m\,V^2$. This is consistent with the difference in kinetic energy before and after the turn. Note that in this example there is no change in potential energy. The change in kinetic energy $= \frac{1}{2}m(2V)^2 - \frac{1}{2}m(0)^2 = 2\,m\,V^2$.

Up until now the assumption was made that the airplane was in vertical equilibrium and therefore the load factor was equal to one. However, there is additional work being done during the turn near a waypoint due to a load factor greater than one. This increased load factor increases drag so it affects the specific excess power in the vicinity of each waypoint where turning occurs. We can create a similar integral to the first term on the right side of equation (3.22). This will be an integral of the difference of the power required for the increased drag and the power required for the level-flight drag over the time it takes to make the turn.

$$\text{Work due to maneuvering drag} = \int_0^{\Delta t} \frac{D(1) - D(n)}{W} V[1 + \mathcal{F}]\,dt \qquad (3.26)$$

where Δt is the time to complete the turn and W is the weight. To find this difference in drag we start with a representation of drag as

$$D = C_D \left(\frac{1}{2}\rho V^2\right) S$$

A parabolic drag polar is being used so

$$C_D = C_{D_o} + k C_L^2 \qquad (3.27)$$

The lift coefficient can be expressed in terms of the load factor (n) as

$$C_L = \frac{nW}{\rho V^2 S/2}$$

From this the drag equation becomes

$$D = \frac{1}{2}\rho V^2 S \left[C_{Do} + k\left(\frac{nW}{\rho V^2 S/2}\right)^2\right] \qquad (3.28)$$

Then the drag in equation (3.28) is subtracted from the drag for a load factor of one and simplified.

$$\begin{aligned}
D(1) - D(n) &= \frac{1}{2}\rho V^2 S k \left[\left(\frac{W}{\rho V^2 S/2}\right)^2 - \left(\frac{nW}{\rho V^2 S/2}\right)^2\right] \\
&= \frac{2kW^2}{\rho V^2 S}(1 - n^2)
\end{aligned}$$

16

Now the integral from equation (3.26) can be evaluated.

$$\text{Work due to maneuvering drag} = \int_0^{\Delta t} \frac{2kW}{\rho V S}(1 - n^2)[1 + \mathcal{F}]\, dt$$

We assume the turn is made in a circular path with respect to the surrounding air so the load factor will be constant. Everything else in the integral will also be constant during the turn except for the $\mathcal{F}$ term so that is all that remains in the integral.

$$\text{Work due to maneuvering drag} = \frac{2kW}{\rho V S}(1 - n^2)\left[\Delta t + \int_0^{\Delta t} \mathcal{F}\, dt\right]$$

After integrating we have the following

$$\text{Work due to maneuvering drag} = \frac{2kW}{\rho V S}(1-n^2)\left[\Delta t + \frac{V_w}{V}\frac{(-\sin(\chi_w - \chi_r) + \sin(\chi_w - \chi_l))}{\dot{\chi}}\right] \tag{3.29}$$

where the subscripts, r and l, refer to the right and left waypoints respectively. While the change in time is not known directly, it can be calculated by dividing the change in heading angle by the heading rate ($\dot{\chi}$). Assuming a horizontal coordinated turn we have

$$\dot{\chi} = \frac{g}{V}\sqrt{n^2 - 1} \tag{3.30}$$

Substituting equation (3.30) into equation (3.29)

$$\begin{aligned}\text{Work due to maneuvering drag} \quad = \quad &-\frac{2kW\sqrt{n^2-1}}{\rho S g}\left[|(\chi_r - \chi_l)|\right. \\ &+ \left.\frac{V_w}{V}|(-\sin(\chi_w - \chi_r) + \sin(\chi_w - \chi_l))|\right]\end{aligned} \tag{3.31}$$

The final energy constraint equation comes from combining the total energy from equations (3.22), (3.25) and (3.31) and using an implicit Euler scheme to approximate the integrals.

$$\begin{aligned}0 \quad = \quad & E_r - E_l \\ & - \quad \Delta t(1 + \mathcal{F}_l)(Ps_r + Ps_l)/2 \\ & + \quad \mathcal{F}_l(h_r - h_l) \\ & + \quad m_r V_r V_{w_r}(\cos(\chi_r - \chi_{w_r}) - \cos(\chi_l - \chi_{w_r})) \\ & - \quad \frac{2kW\sqrt{n^2-1}}{\rho S g}(|\chi_r - \chi_l| \\ & + \quad \frac{V_{w_r}}{V_r}|\sin(\chi_{w_r} - \chi_l) - \sin(\chi_{w_r} - \chi_r)|)\end{aligned} \tag{3.32}$$

3.3   Mass Change Constraint

The final equality constraint is an integral form of equation (A.24). This requires that the change in weight between adjacent waypoints equal to the integral of the fuel-rate. The

17

fuel- rate is dependent on the specifics of the engine. In this case those details are outlined in Appendix C. We have

$$m_r - m_l + \int \dot{W}_f \, dt \; = \; 0.$$

As before, we use an implicit Euler scheme to approximate the integral in terms of data values at the adjacent waypoints.

$$m_r - m_l + \frac{\Delta t}{2}(\dot{W}_{f_r} + \dot{W}_{f_l}) \; = \; 0. \tag{3.33}$$

The flight time is given by (3.2).

Chapter 4

Vertical Plane Flight Numerical Results

A code was written which uses simplified vertical plane versions of the constraints from the previous chapter. Several problems were run on this version of the code for a few reasons. First of all this is a simpler case and was used to see if the results made sense. Secondly head winds and tail winds were introduced to see how they affect the flight path.

4.1   Description of Problem

The states are range, x, energy, E, and mass, m. The controls in the problem are altitude, h, and throttle setting, ξ. Since the energy can be computed from equation (3.11) we include the vehicle's velocity with respect to the surrounding air mass in the analysis.

The NLP problem was set up in the following manner. The range coordinates were kept in a separate array and are not available to the optimization algorithm. It is convenient to arrange the remaining flight variables in a matrix. Each column of the matrix contains the relevant variables at a waypoint. The variables marked with an * are the optimization variables while the rest are fixed by the boundary conditions.

$$X = \begin{bmatrix} x_0 \ x_1 \ \ldots \ x_{N_p} \end{bmatrix}$$

$$A = \begin{bmatrix} h_1 & *h_2 & \ldots & h_{N_p} \\ V_1 & *V_2 & \ldots & V_{N_p} \\ m_1 & *m_2 & \ldots & *m_{N_p} \\ *\xi_1 & *\xi_2 & \ldots & *\xi_{N_p} \end{bmatrix} \tag{4.1}$$

The optimization was subject to energy and mass constraints between every waypoint. A simplified version of equation (3.32) is used for the energy constraint. Since the flight

is restricted to a vertical plane, the turning section of the energy constraint is not needed. Now $\mathcal{F} = \frac{V_w}{V}$ where both V_w and V are positive in the positive x direction.

$$
\begin{aligned}
0 \;=\;& E_r - E_l \\
&-\; \Delta t(1 + \mathcal{F}_l)(Ps_r + Ps_l)/2 \\
&+\; \mathcal{F}_l(h_r - h_l)
\end{aligned}
\tag{4.2}
$$

The mass constraint is the same as equation (3.33). With these two constraints the following summarizes the numbers of waypoints, variables, constraints, and degrees of freedom in the NLP problem.

- N_p waypoints

- $4 \cdot (N_p - 2) + 3$ variables

- $2 \cdot (N_p - 1)$ equality constraints

- $2 \cdot N_p - 3$ degrees of freedom

For our numerical studies there are 29 waypoints, so there are 111 optimization variables, 56 constraints, and 55 degrees of freedom.

The time from one waypoint to the next is calculated by dividing the distance traveled by the average inertial velocity at which the aircraft flies.

$$
x_{i+1} - x_i - \int V_h \, dt \;=\; 0.
\tag{4.3}
$$

The integral is approximated as

$$
\int V_h \, dt \;=\; \frac{V_h(i+1) + V_h(i)}{2} \Delta t
\tag{4.4}
$$

which is substituted into equation (4.3) and solve for Δt. The throttle setting, ξ, must remain between 0.1 and 1 while the altitude, h, had a lower bound of 0.

All the results were run for the case of flying from $x = -4000$ nmi to $x = 0$ nmi over a fixed grid of points. The initial condition on altitude was 10,000 feet while the initial condition on velocity was 150 ft/sec. There are final conditions imposed which bring the vehicle back to the initial velocity and altitude. As mentioned in Chapter 1 the performance index was a linear combination of the weight of fuel consumed and the total flight time, $J = W_f + \mu \, t_f$ where $\mu \geq 0$.

4.2 Results

Figures 4.1 through 4.4 are the results of running the vertical plane version of the code with no winds and varying the parameter, μ, in the cost function ($J = W_f + \mu\ t_f$). As emphasis on time increases, the total time to fly decreases and the plane uses more fuel because it has a higher throttle setting for a greater percentage of the flight. In Figure 4.2 (intermediate μ) and Figure 4.3 (large μ) the throttle stays at 100% even after the airplane starts to descend, using both gravity and maximum power for more speed.

At the fifteenth waypoint on Figure 4.1, $h = 76,400$ ft and the weight is 4942 lb. From equation (B.3) the minimum drag velocity is found to be 416.9 ft/sec at that altitude and weight. From the optimal solution, the velocity at the fifteenth waypoint is actually 416.9 ft/sec so the airplane is flying at the minimum drag velocity. The data at the rest of the waypoints for this case with no winds and no emphasis on time reveal similar results.

Figure 4.4 shows the family of solutions mentioned in the Introduction. It was constructed by taking final times and final fuel consumed from the cases run while varying μ. It should be noted that only the points marked with a 'plus' sign in the figure are from actual data. The lines drawn between them are not from data but are only there to better illustrate the general behavior exhibited by varying the emphasis on time. This figure shows that as μ increases from 0 to 2.26 lb/sec, the flight time decreases from about 22 hours to about 16 hours. The final weight also decreases from 4600 lbs to about 4420 lbs. The final weight decreases because more fuel is used when the throttle is at 100% for a greater portion of the flight as μ increases.

Figures 4.5 through 4.8 are the results of running the code with a tail wind of 50 ft/sec and varying the emphasis on time in the cost function. By applying the same analysis as the case with no winds to find the minimum drag velocity, the eighth waypoint on Figure 4.5 is found to have $u \equiv V/V_{md} = 0.926$ so the plane is flying at less than the minimum drag velocity. This is characteristic of all of the waypoints in this case with a constant tail wind and no emphasis on time.

Figures 4.9 through 4.12 are the results of running the code with a head wind of 50 ft/sec and varying the emphasis on time in the cost function. Waypoint number fifteen on Figure 4.9 is at $u = 1.016$ so the vehicle is flying slightly above the velocity for minimum drag and this is typical of the entire flight. By looking at Figures 4.4, 4.8, and 4.12, it is obvious that as the wind against the airplane increases, the range of possible flight times decreases.

These vertical plane results took from 9 seconds to 55 seconds on a DEC Alpha 2100 computer system. In general the run time was shorter as the emphasis on time increased.
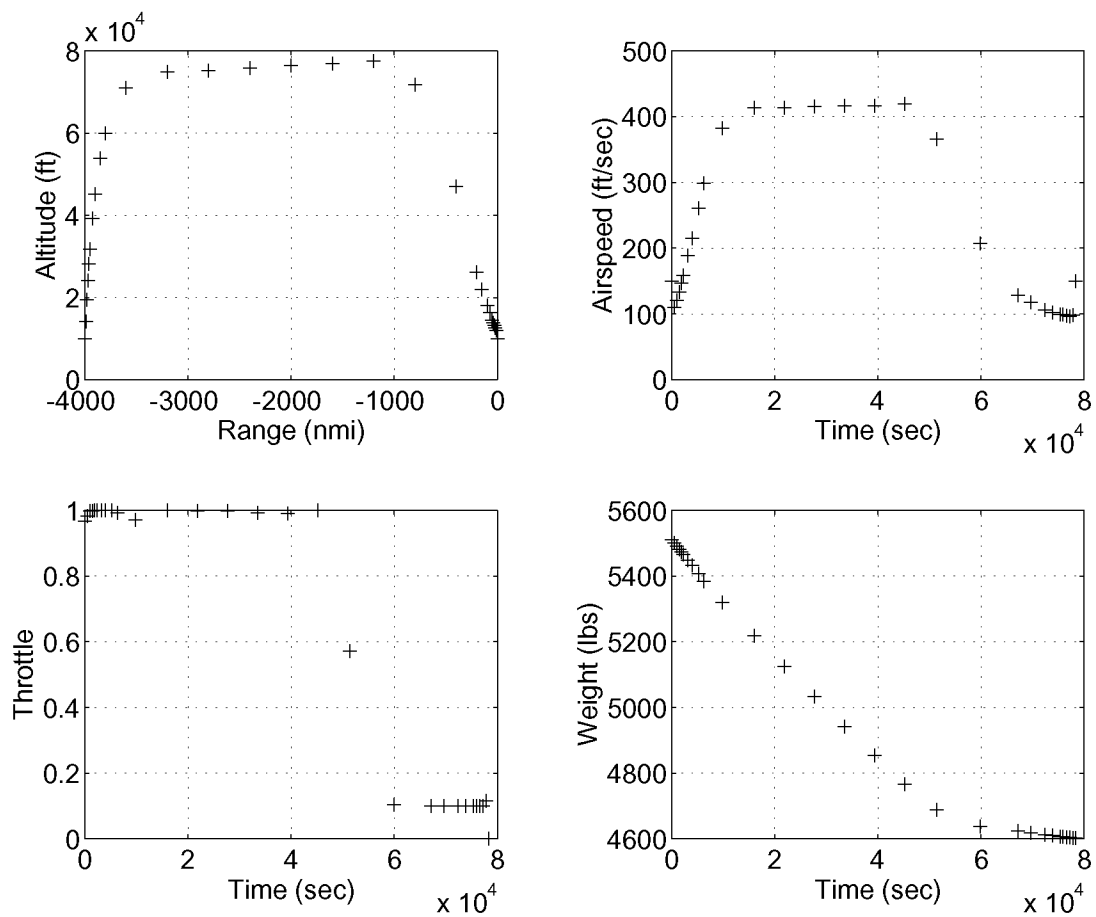
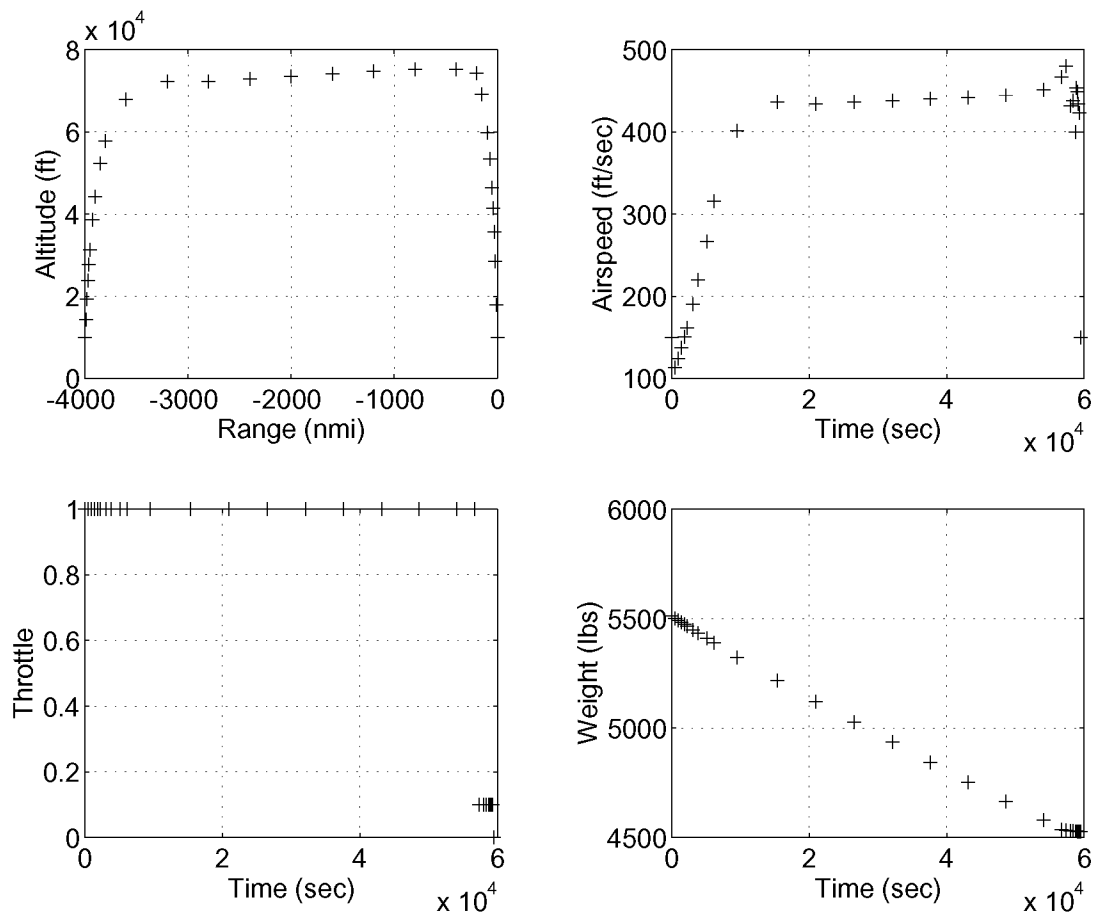21

Figure 4.1: Vertical Plane, Winds = 0, $\mu = 0$

Figure 4.2: Vertical Plane, Winds = 0, $\mu = 0.0226$ lb/sec
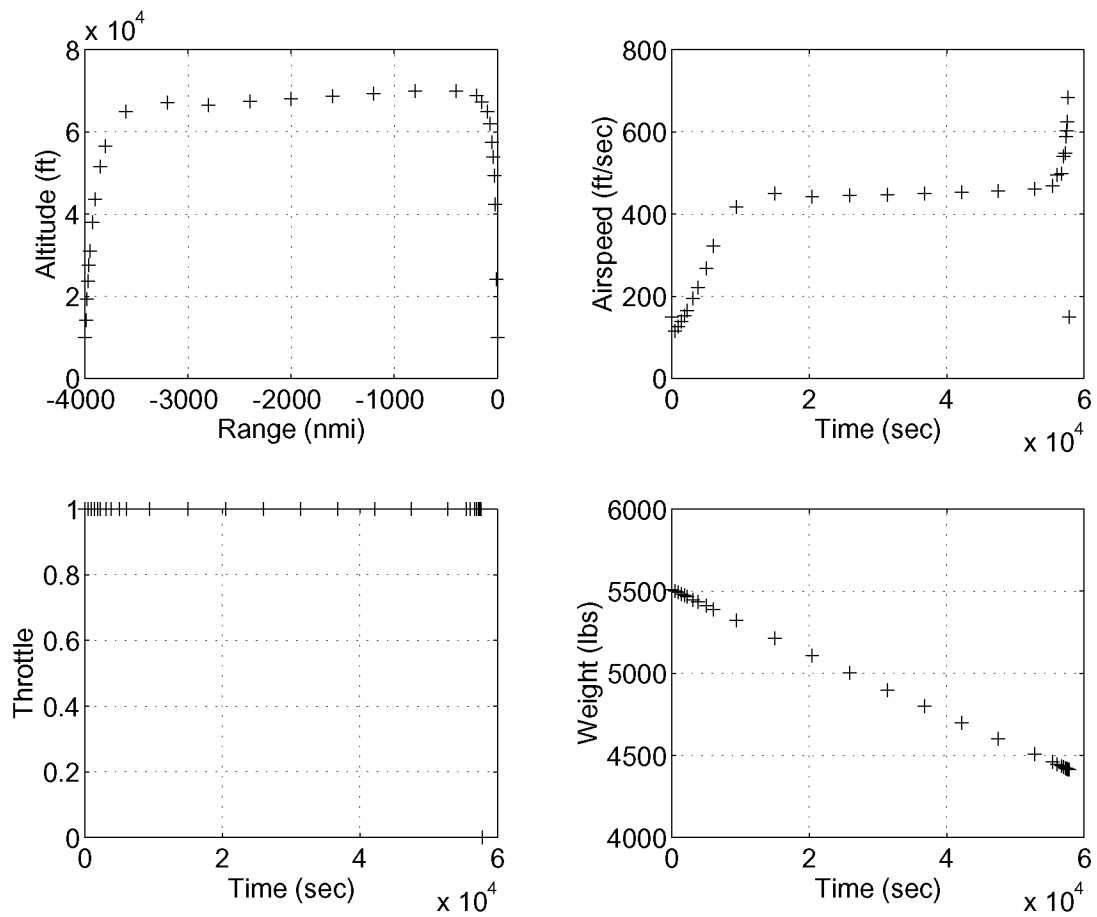
23

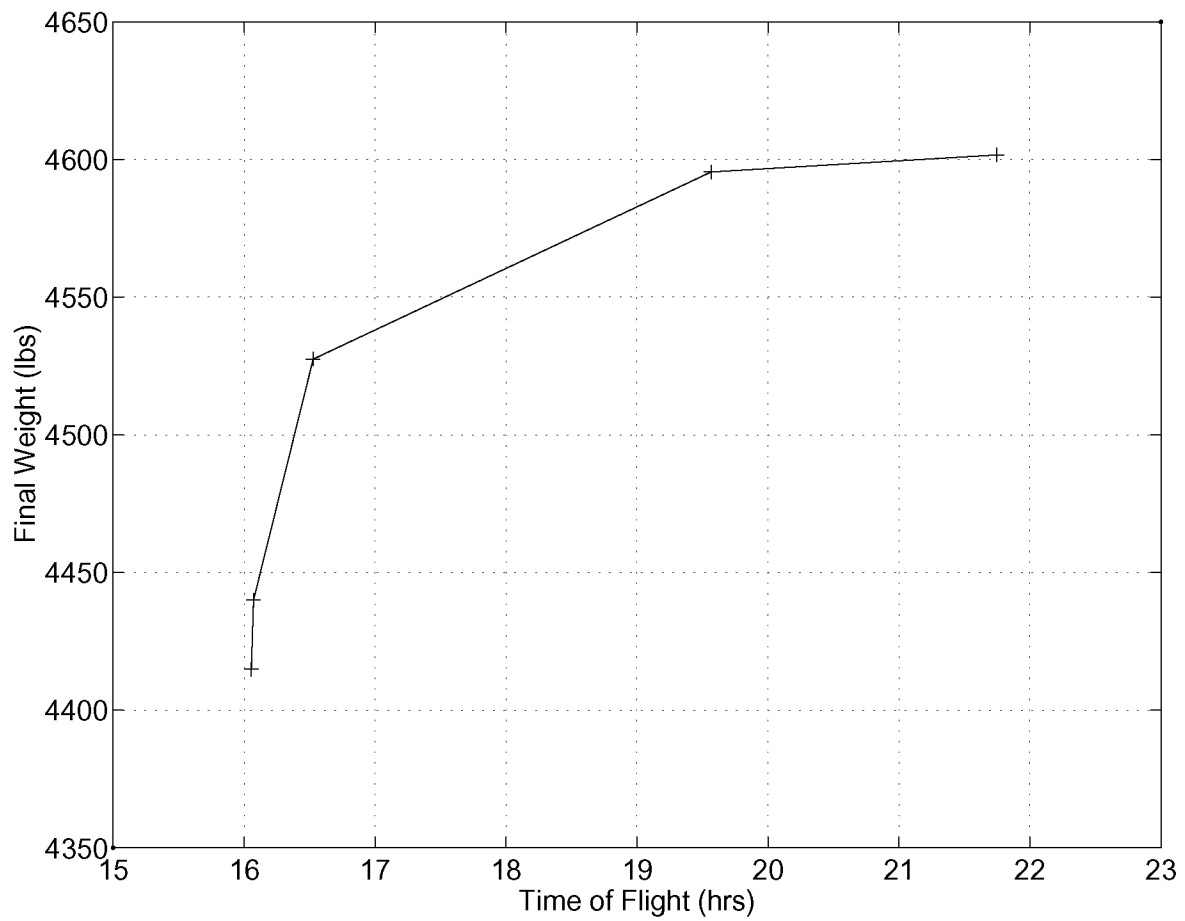Figure 4.3: Vertical Plane, Winds = 0, μ = 2.26 lb/sec

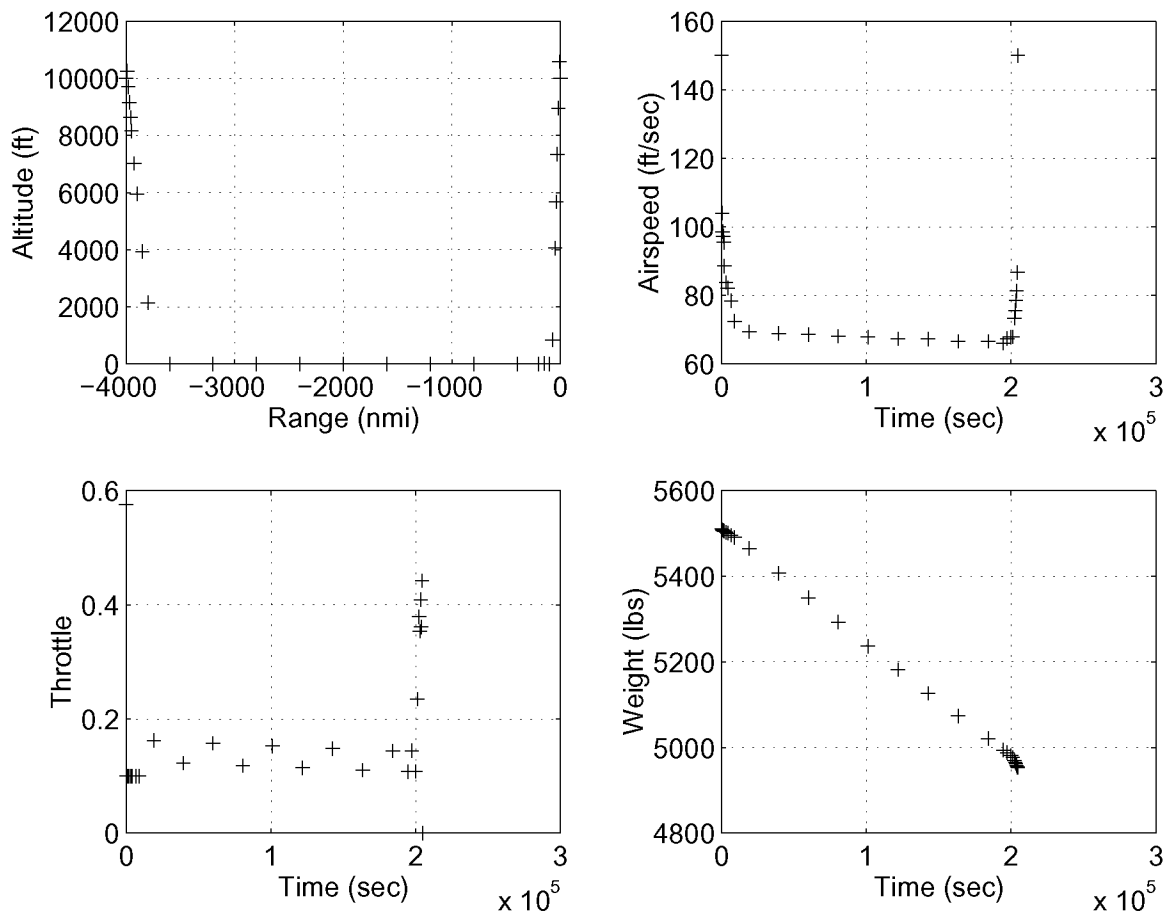Figure 4.4: Vertical Plane Family of Solutions, Winds = 0 ft/sec

Figure 4.5: Vertical Plane, Tail Wind $= 50$ ft/sec, $\mu = 0$
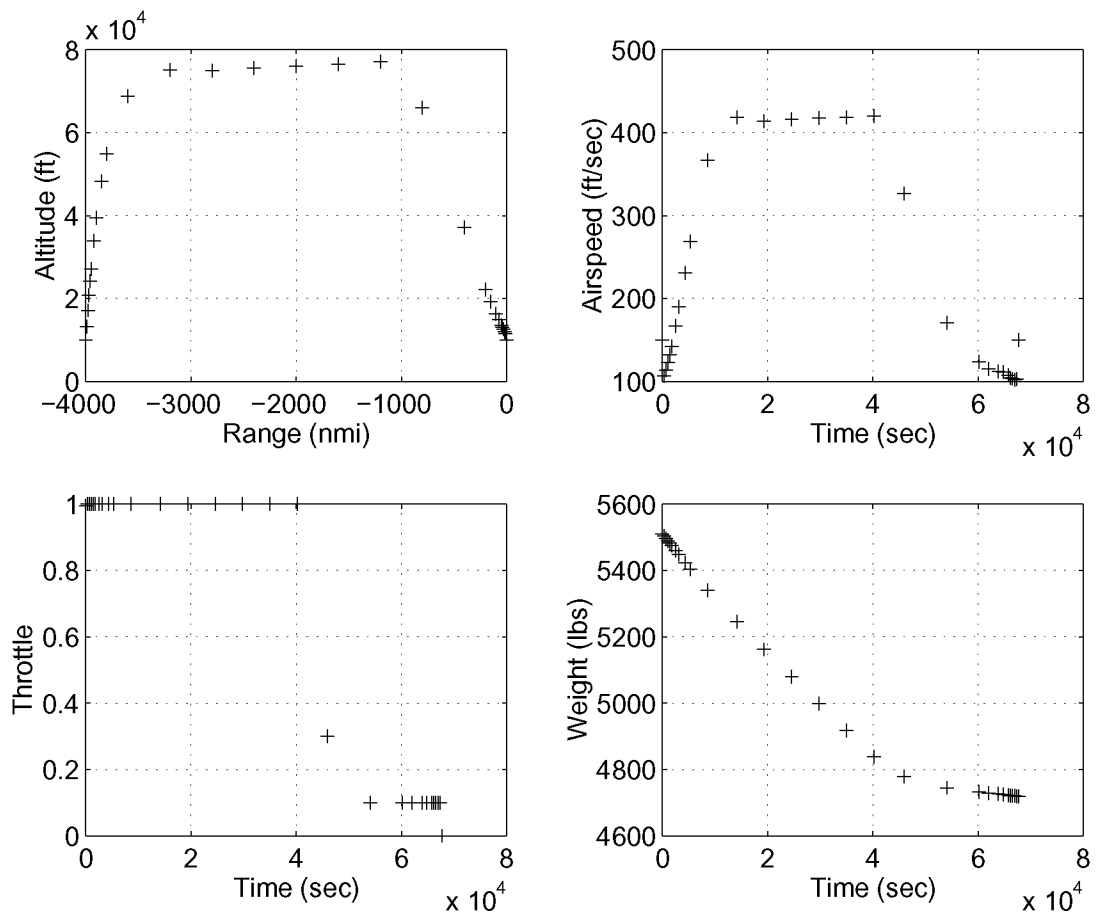
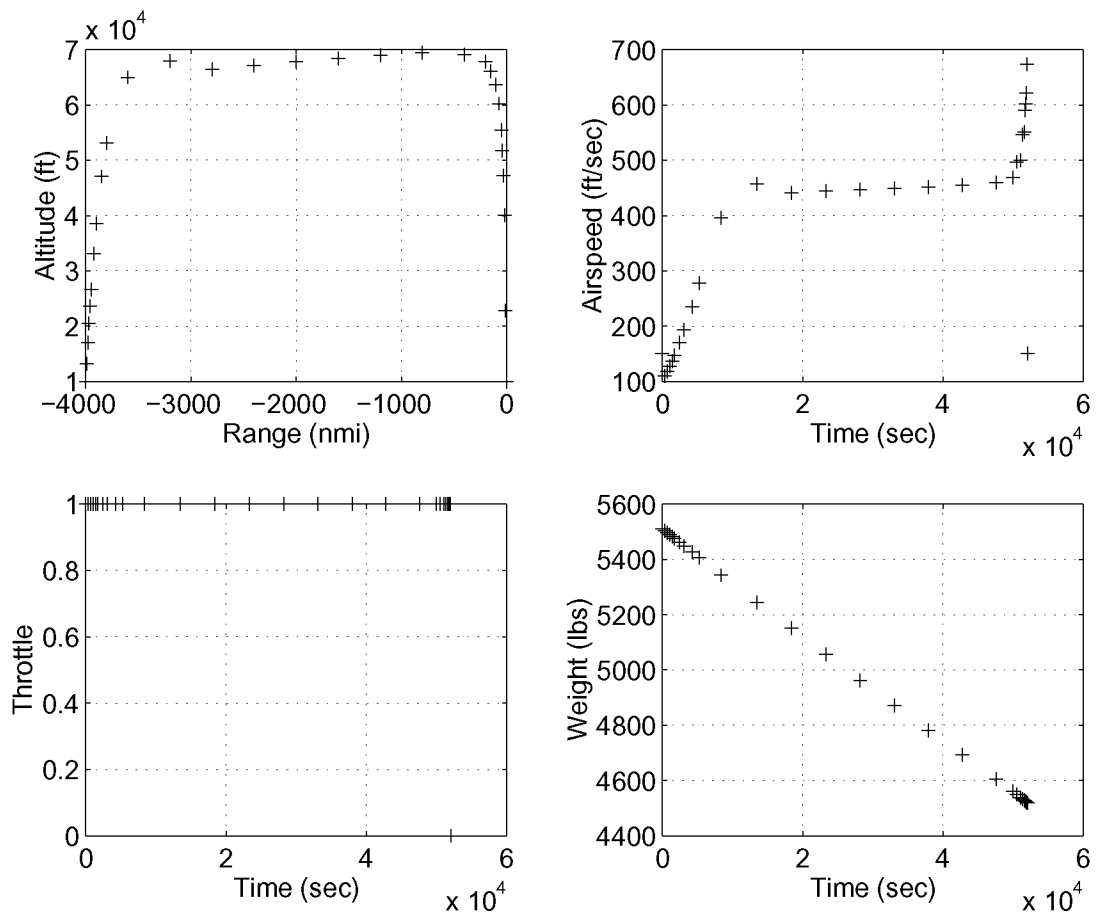Figure 4.6: Vertical Plane, Tail Wind = 50 ft/sec, $\mu = 0.00226$ lb/sec

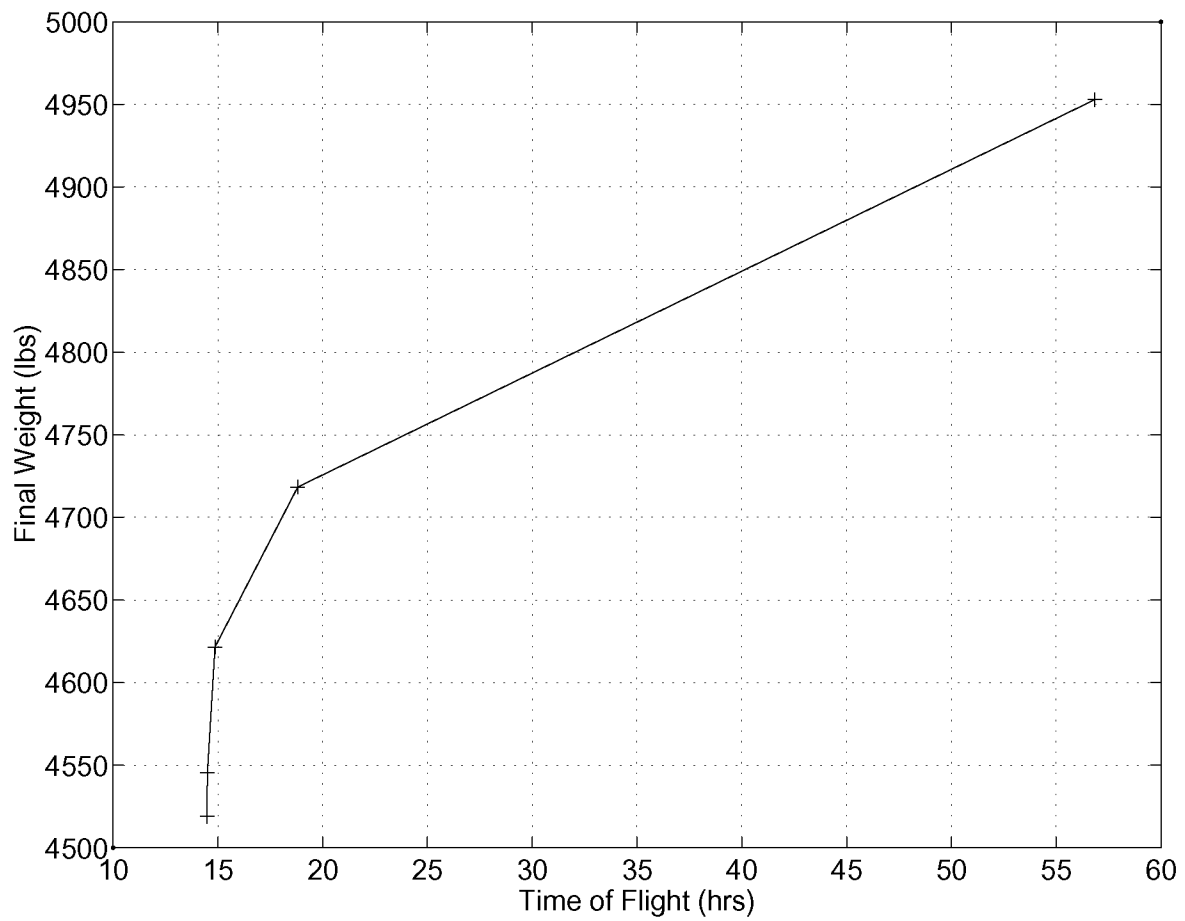Figure 4.7: Vertical Plane, Tail Wind = 50 ft/sec, $\mu = 2.26$ lb/sec

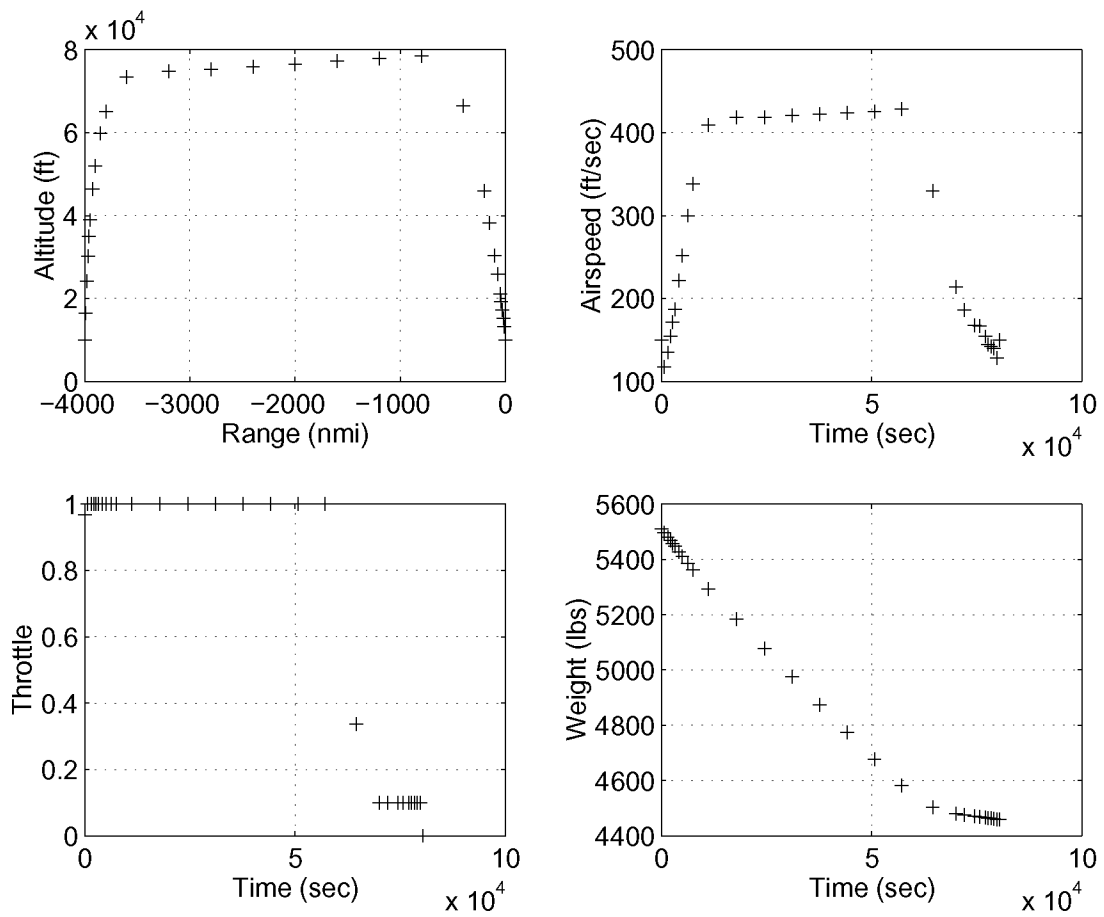Figure 4.8: Vertical Plane Family of Solutions, Tail Wind = 50 ft/sec

Figure 4.9: Vertical Plane, Head Wind = 50 ft/sec, $\mu = 0$
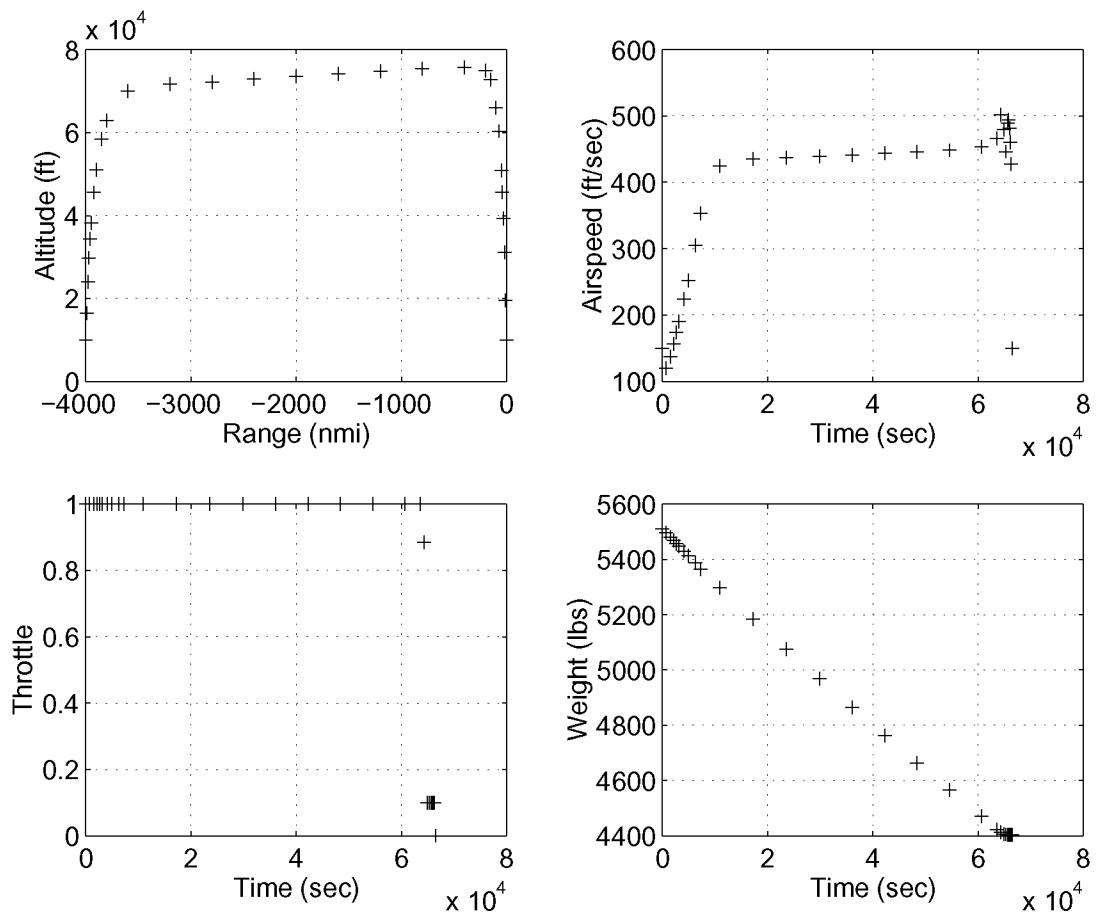
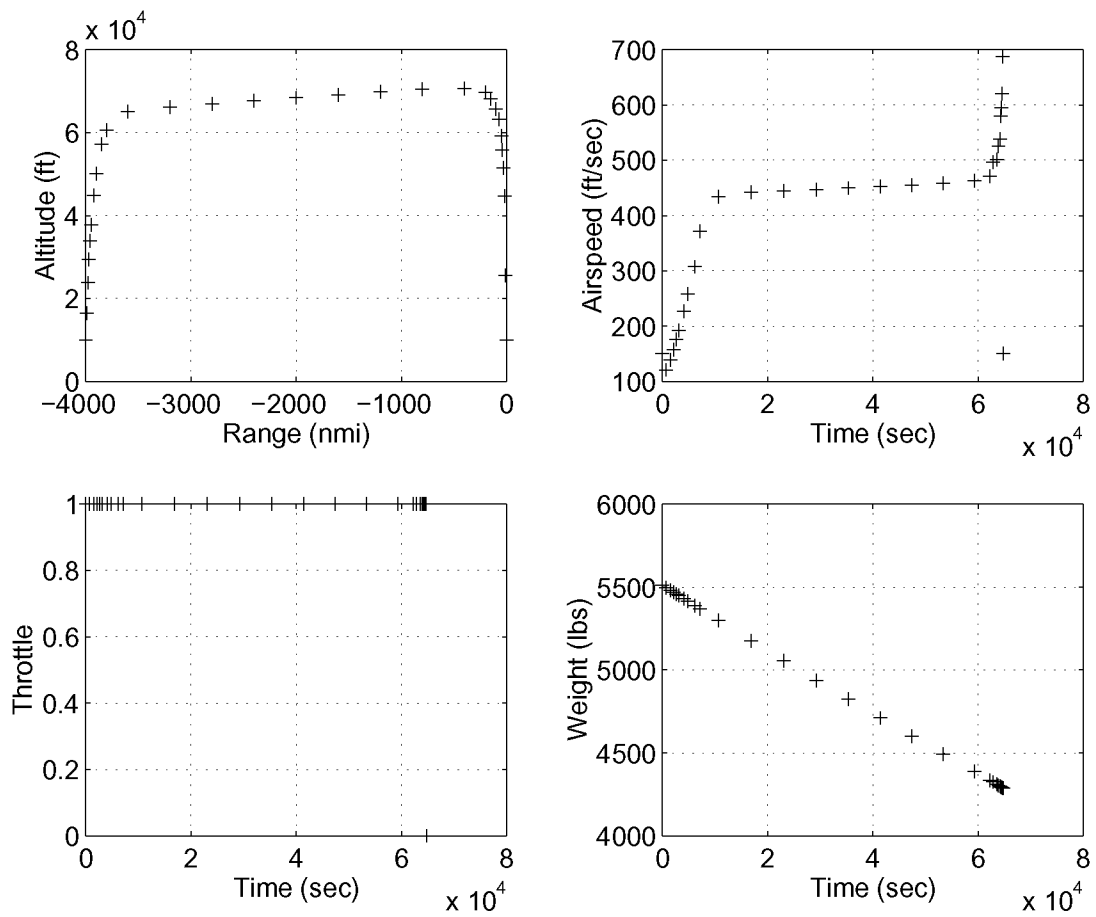Figure 4.10: Vertical Plane, Head Wind = 50 ft/sec, $\mu = 0.0226$ lb/sec

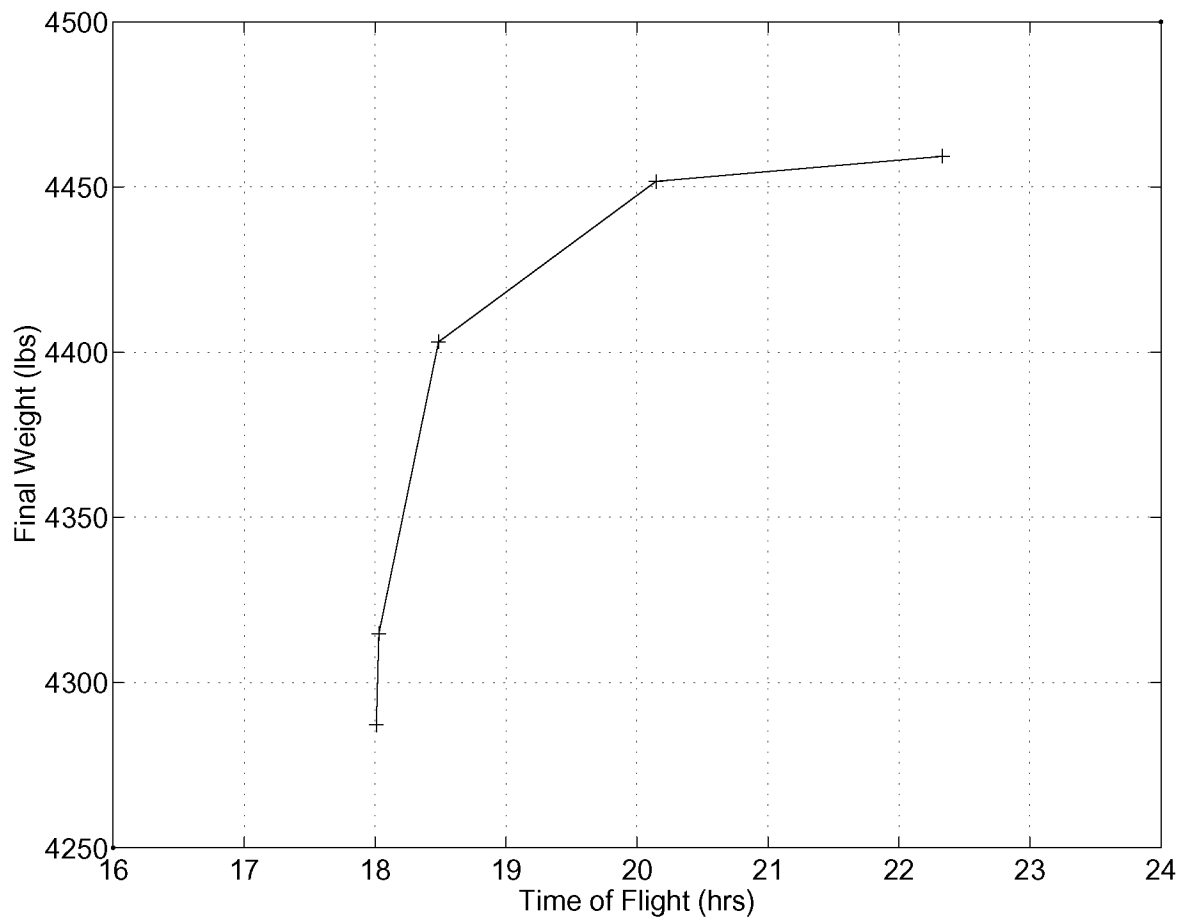Figure 4.11: Vertical Plane, Head Wind = 50 ft/sec, $\mu = 2.26$ lb/sec

Figure 4.12: Vertical Plane Family of Solutions, Head Wind = 50 ft/sec

Chapter 5

Three Dimensional Flight Numerical Results

5.1 Description of Problem

The states in this three-dimensional problem are horizontal position coordinates, x and y, energy, E, and mass, m. The controls in the problem are altitude, h, throttle setting, ξ, and heading, χ. As before, the path is parameterized in terms of flight speed and the energy is computed from equation (3.11).

The path is approximated by specifying at each waypoint the seven values: $(x, y, h, V, m, \chi, \xi)$. Between each adjacent pair of waypoints we enforce the equality constraints from kinematics (3.3); from energy (3.32) and from mass change (3.33). In addition, we have the inequality constraint (3.4). The bounds on the controls are the same as those for the vertical plane problem in the previous chapter. For a simple flight problem we suppose that the values of the first five variables are specified at the initial point and that the final values of the horizontal position, velocity and heading angle are specified. The rest of the variables, each denoted by an asterick in equation (5.1), are the optimization variables.

In this three dimensional problem the horizontal coordinates cannot be held constant over the entire flight as they were in the vertical plane problem because turning at the waypoints must be allowed to occur so all of the variables are conveniently viewed in one matrix, A.

$$A = \begin{bmatrix} x_1 & *x_2 & \dots & x_{N_p} \\ y_1 & *y_2 & \dots & y_{N_p} \\ h_1 & *h_2 & \dots & h_{N_p} \\ V_1 & *V_2 & \dots & V_{N_p} \\ m_1 & *m_2 & \dots & *m_{N_p} \\ *\chi_1 & *\chi_2 & \dots & \chi_{N_p} \\ *\xi_1 & *\xi_2 & \dots & *\xi_{N_p} \end{bmatrix} \qquad (5.1)$$

with

- N_p waypoints

- $7 \cdot (N_p - 2) + 4$ variables

- $3 \cdot (N_p - 1)$ equality constraints

- $4 \cdot N_p - 7$ degrees of freedom

For our numerical studies there are 15 waypoints so there are 95 optimization variables, 42 constraints, and 53 degrees of freedom. For this three dimensional problem winds are always horizontal in a counterclockwise direction about the origin. The problem will start at some distance from the origin at a high altitude with some approximated amount of fuel left to simulate the aircraft at the end of the data-taking leg of the mission. The results from the previous chapter can be used to approximate how much fuel will be left after taking data. In all cases in this chapter 1000 lbs of fuel will be the amount said to have been consumed before heading home. All of the constraints are used as they are derived in Chapter 3. There is also an inequality constraint (3.4) to keep the waypoints from getting too close together.

The problem was solved for two main cases of initial position as seen in Figure 5.1. The first case starts at point A where $x = 0$ nmi and $y = -1000$ nmi and the second starts at point B with $x = 0$ nmi and $y = 1000$ nmi. The final destination is always at $x = -2800$ nmi and $y = 0$ nmi. The airplane is started at an altitude of 60,000 ft, since it will be at a high altitude when completing the science mission. There are final conditions imposed which bring the vehicle to an altitude of 10,000 ft and an airspeed of 150 ft/sec.

The problem is run with two different models. The first is an analytic model with wind speeds varying as in Figure 5.2. The winds increase linearly with distance from the Pole and piecewise linearly with altitude and they are circulating west to east about the Pole. The maximum wind speed is 100 ft/sec which occurs 2800 nmi from Pole above 40,000 feet. The first few results are with the start of flight at point A and varying μ, the emphasis on time in the cost function. A second case will start at point B also varying μ. The second wind model is a cubic spline fit of wind data obtained from the NASA Goddard Space Flight Center (GSFC). In this model the winds are still horizontal only and they are also circulating west to east about the Pole. The data is taken from average daily values, and wind speed is described as a function of distance from the Pole (latitude) and altitude. The wind field from $-40°$ to $-90°$ latitude is pictured in Figure 5.3. Since data is only available between altitudes of about 18,300 feet and 102,000 feet, the initial altitude in these problems is 60,000 feet as before but the final altitude is 19,000 feet. The performance index was the same linear combination of the weight of fuel consumed and the total flight time, $J = W_f + \mu\, t_f$ as in Chapter 4.
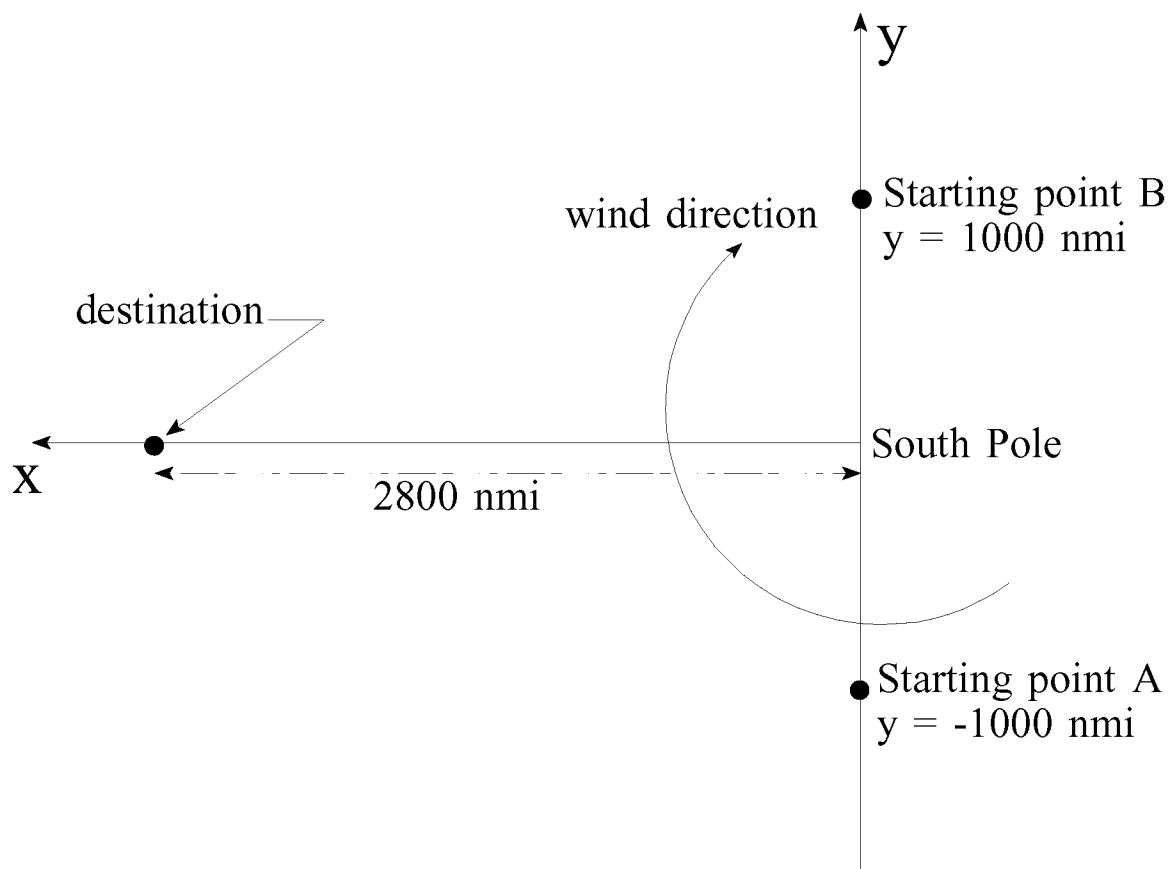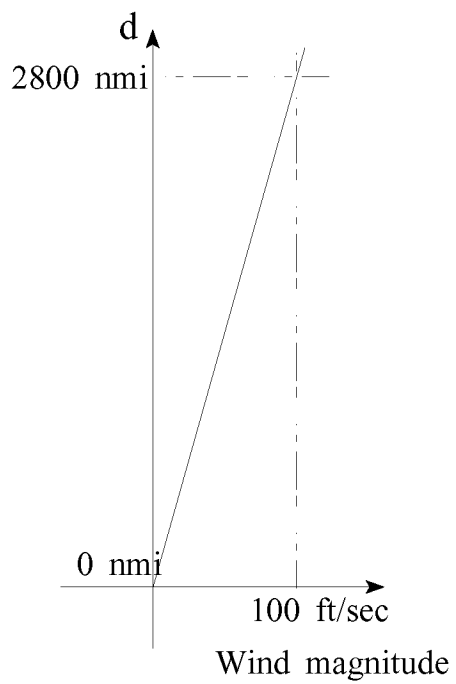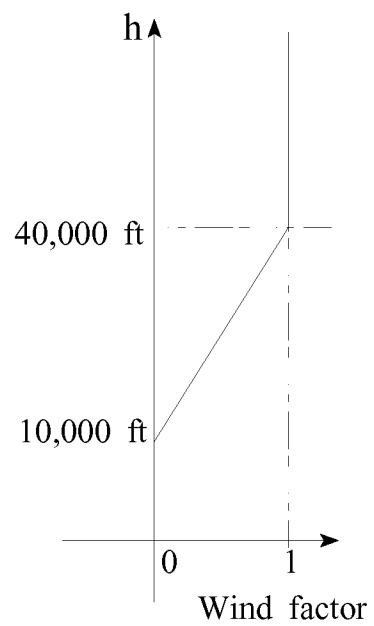
Figure 5.1: Horizontal Projection of Three Dimensional Problem

Figure 5.2: Winds Varying with Range and Altitude
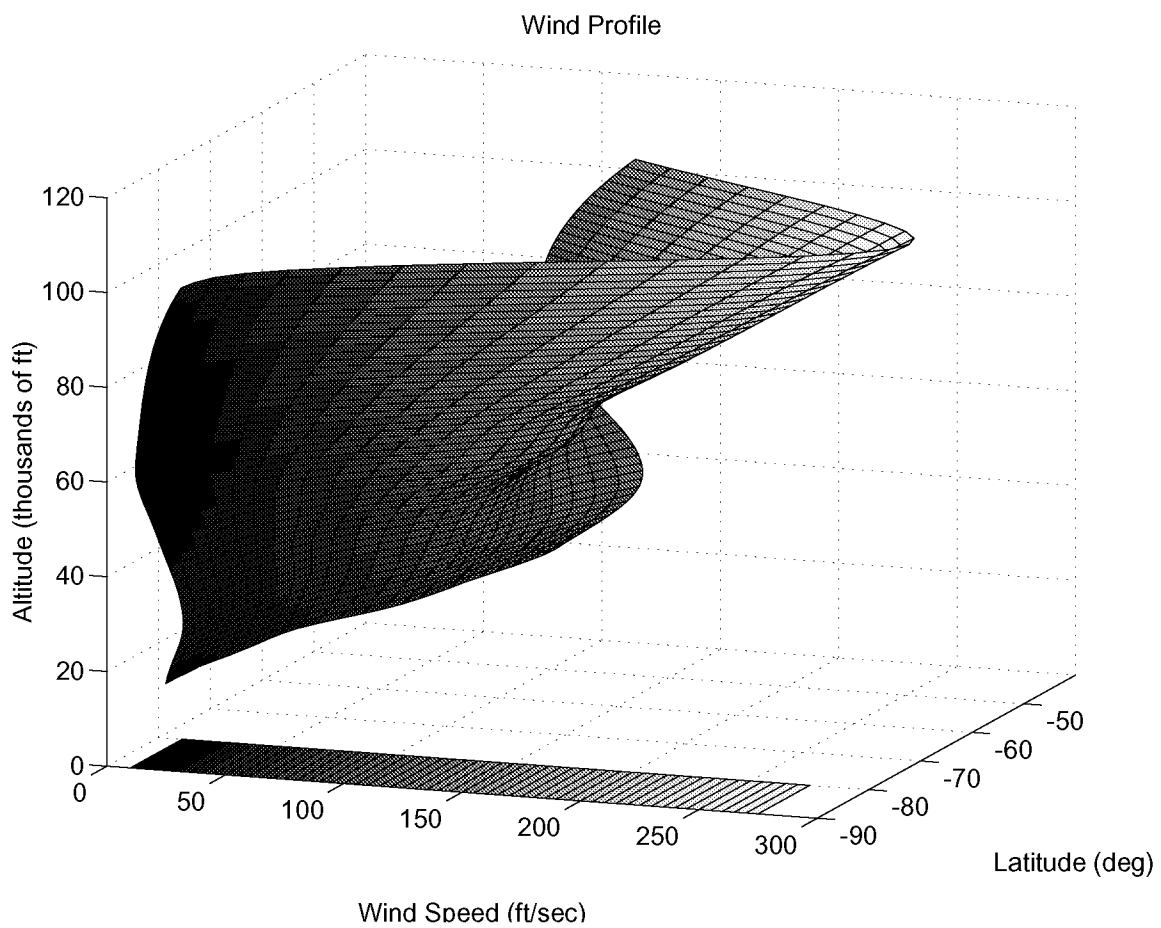
Wind Profile

Figure 5.3: NASA GSFC Wind Model

5.2 Results

Figure 5.4 shows the horizontal projections of the results with $\mu = 0$ and $\mu = 3.048$ lb/sec with the flight beginning at point A in Figure 5.1. With this starting point the direction of the wind is helping the vehicle return to the base. Other intermediate cases were run and are discussed later but only the extreme cases are shown in this figure for clarity. The short line vectors coming from each waypoint, denoted by a circle, shows the heading of the airplane with respect to the surrounding air. With $\mu = 0$ or a small number the airplane starts its flight by almost turning away from the destination to fly a more curved path. This maneuver is made to allow the circulating winds to help later in the flight. As μ is increased the airplane takes a more direct path to its destination.

Figures 5.5 through 5.7 show range histories of altitude and time histories of velocity, throttle setting, and weight obtained by varying the emphasis on time with the flight beginning at point A. With $\mu = 0$ in Figure 5.5 the altitude does not drop below 40,000 ft for most of the flight since this is the minimum altitude where the winds remain at their maximum for the given range. In the same figure some oscillation in the throttle setting is apparent. This oscillation will be discussed in the Summary and Conclusions Chapter. These figures show that as μ increases in Figures 5.6 and 5.7, the throttle is near 100% for a greater portion of the flight just as for the vertical plane results.

Figure 5.8 shows the time - fuel performance trade-off. This type of plot can be very useful when deciding which path to use depending on time constraints. As noted in the Introduction, operational issues are expected to dictate arrival times. If the vehicle needs to be back as soon as possible, due to an approaching storm for example, one of the paths at the lower left of the plot should be chosen. It should be noted that this figure shows that there is a definite limit to how fast the plane can return home. The code can produce solutions which use more fuel by increasing the emphasis on time in the performance index but the time to return home will not decrease anymore past a certain point. This is because the throttle is already at 100% for the entire flight. There will also be conditions where it may be possible for the vehicle to get home faster but if it tries it may run out of fuel before it gets there. Of course if the operator is not worried about the time of arrival, he should choose a path at the right hand side of the plot to minimize fuel used, and so provide a fuel margin.

Figure 5.9 shows the horizontal projections of the results with $\mu = 0$ and $\mu = 3.048$ lb/sec with the flight beginning at point B in Figure 5.1. Now the circulating winds are mainly against the direction of the flight. The top curve in this figure is the one for $\mu = 0$. The sharp turn at the third to the last waypoint is where the plane dropped below 10,000 ft (there are no winds). This is why the heading is in the same direction as the actual flight path for the last few waypoints. Figures 5.10 through 5.12 show results with varying the emphasis on time with the flight beginning at point B. These figures show that as μ increases, the throttle is near 100% for a greater portion of the flight just as for the vertical

39

plane results. Figure 5.13 shows the performance trade-off. This time there is a smaller range of times (between 12 and 23 hours) to return the plane to the base.

These three dimensional results took from 4 seconds to 30 seconds on a DEC Alpha 2100 computer system. As in the vertical plane cases, in general the run time was shorter as the emphasis on time increased.

Figures 5.14 through 5.18 show results using the NASA GSFC wind model (Figure 5.3) starting at point B. In this case the code was run with the wind magnitudes at 50% the value in Figure 5.3 because in several of the cases the airplane was not able to return to the base with the given amount of fuel in those high winds.

With this much variability in the wind speeds with altitude and latitude there is the possibility of local minima. However, this possibility was not considered in this analysis. In the future a variety of initial guesses on the variables can be used to try to explore the possibility of local minima. The results are similar to those using the analytic model.

Figure 5.14 shows that there isn't much variation in the horizontal projections of the paths when μ is varied from 0 to a large number. As in using the analytical wind model, Figures 5.15 through 5.17 show the throttle setting staying at its maximum of unity for a greater portion of the flight, time decreasing, and final weight decreasing as μ increases. Figure 5.18 shows that there is a smaller range of flight times, between 11.75 and 14.5 hours, in the family of solutions.

Figure 5.4: Horizontal Projections of Flight Paths with Varying μ, Starting Point A, Analytic Wind Model

Figure 5.5: 3-D, Starting Point A, $\mu = 0$, Analytic Wind Model

Figure 5.6: 3-D, Starting Point A, $\mu = 3.048$ lb/sec, Analytic Wind Model

Figure 5.7: 3-D, Starting Point A, $\mu = 3.048$ lb/sec, Analytic Wind Model

Figure 5.8: 3-D Family of Solutions, Starting Point A, Analytic Wind Model

Figure 5.9: Horizontal Projections of Flight Paths with Varying μ, Starting Point B, Analytic Wind Model

Figure 5.10: 3-D, Starting Point B, $\mu = 0$, Analytic Wind Model

47

Figure 5.11: 3-D, Starting Point B, $\mu = 3.048$ lb/sec, Analytic Wind Model

Figure 5.12: 3-D, Starting Point B, $\mu = 3.048$ lb/sec, Analytic Wind Model

49
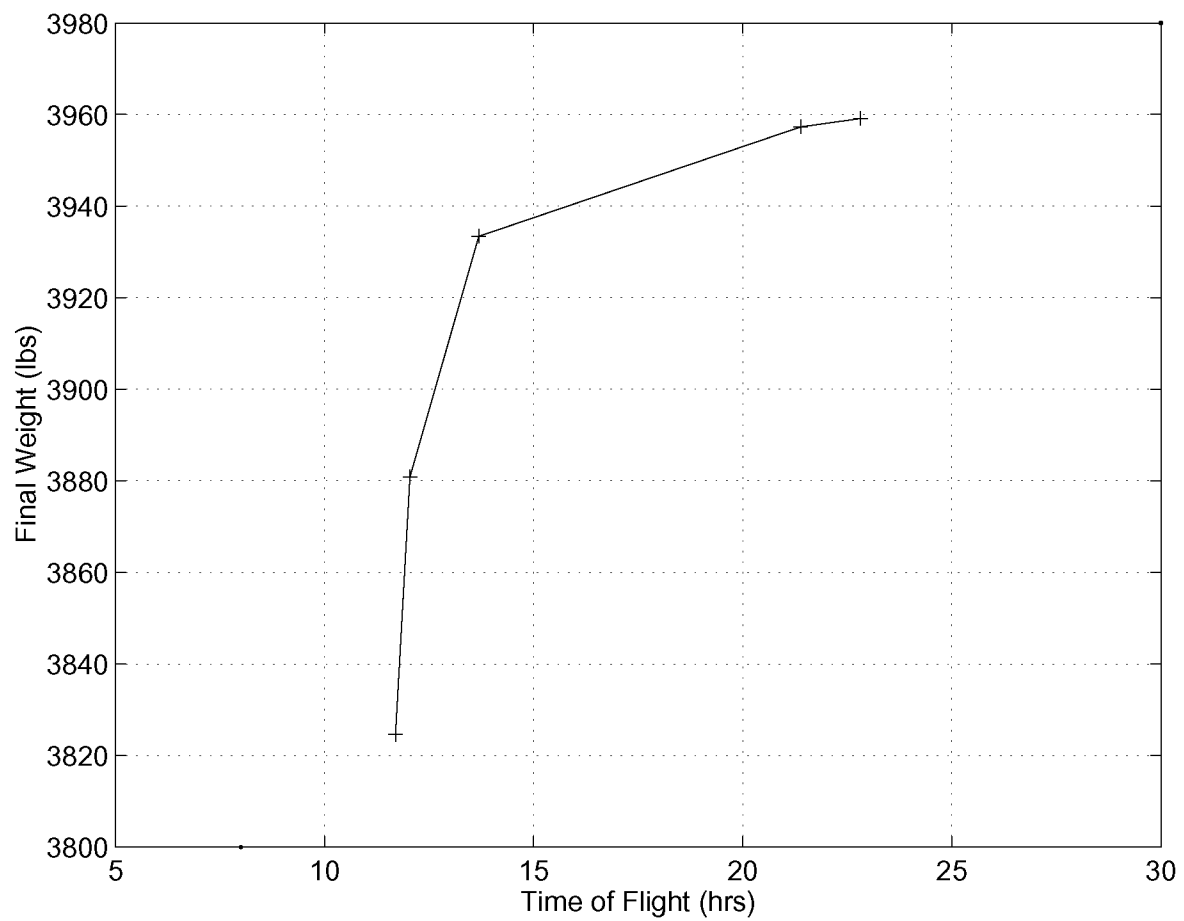
Figure 5.13: 3-D Family of Solutions, Starting Point B, Analytic Wind Model
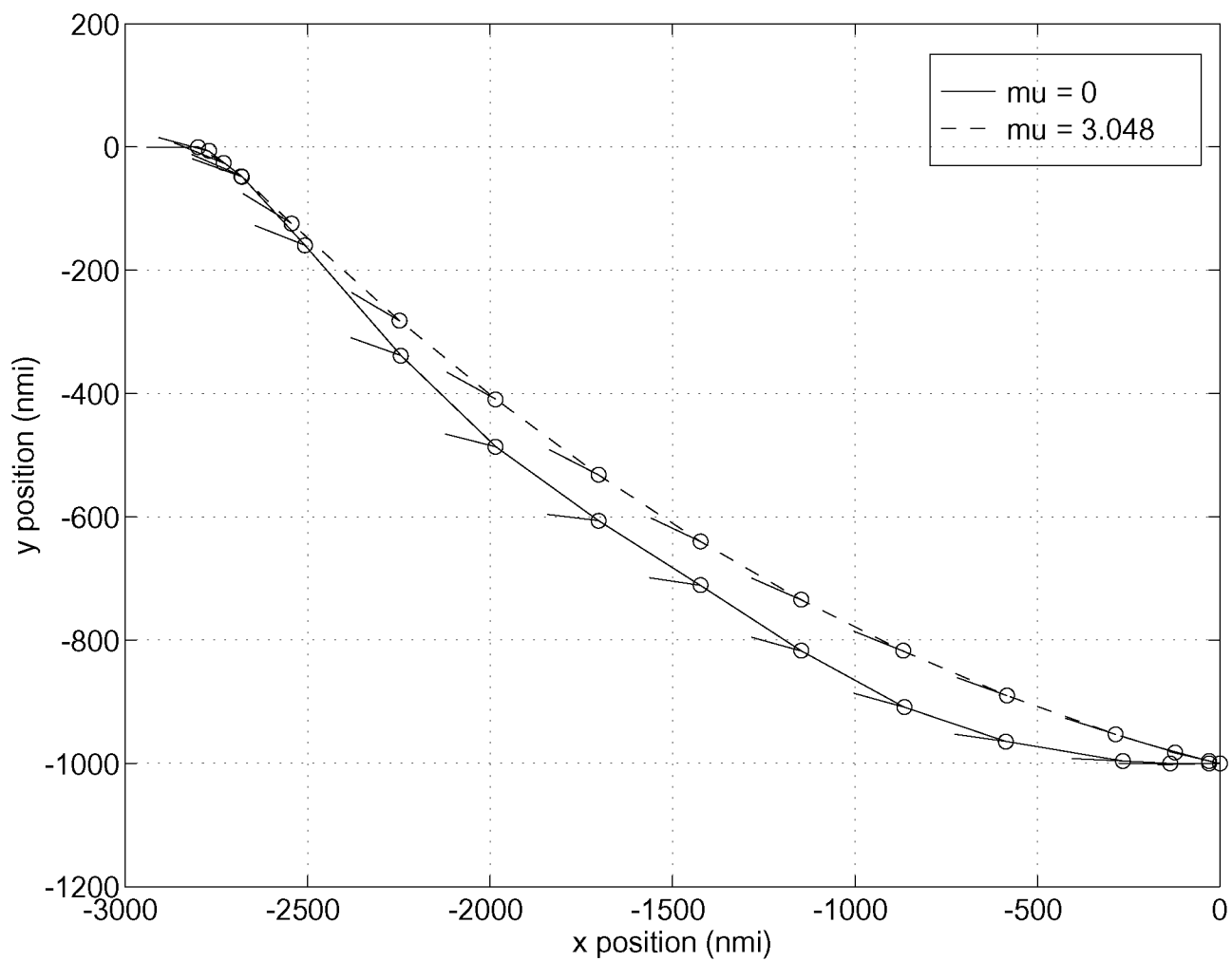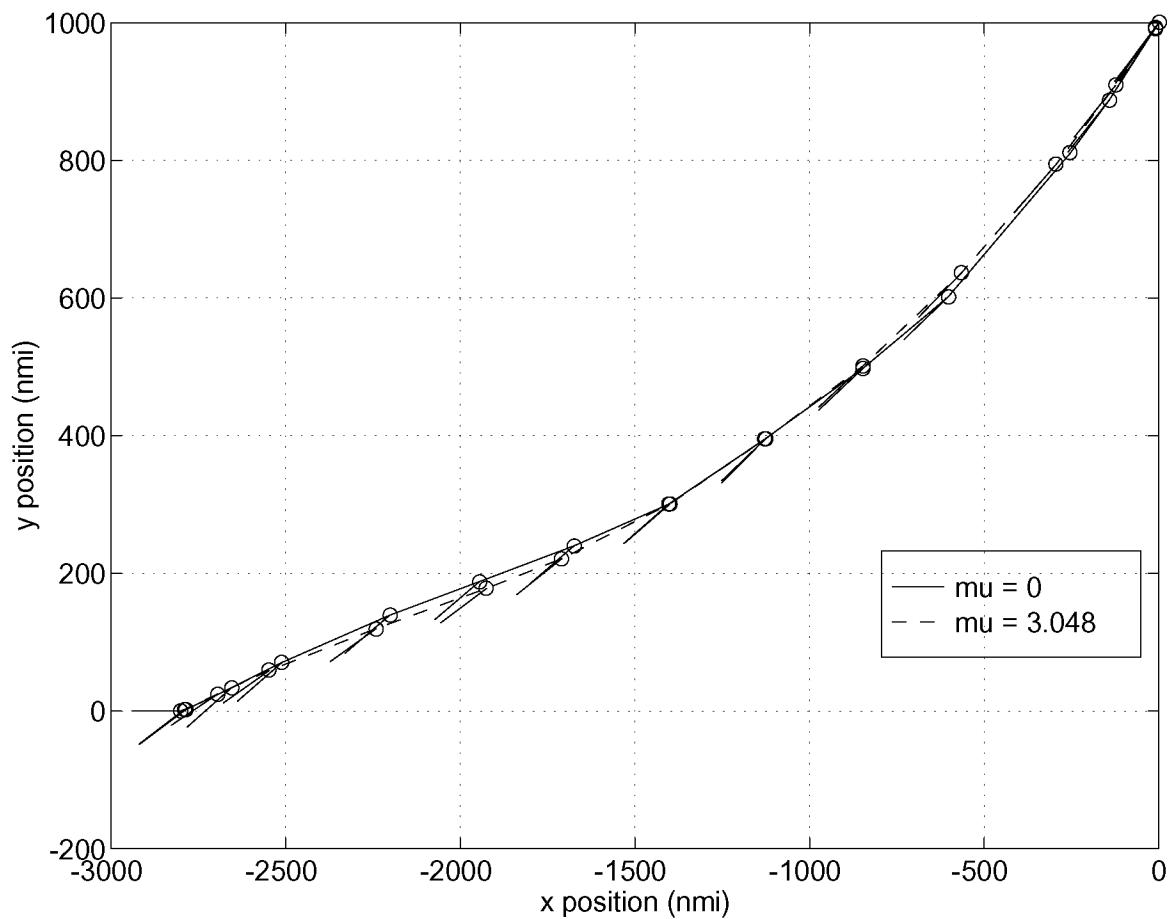
Figure 5.14: Horizontal Projections of Flight Paths with Varying μ, Starting Point B, GSFC Wind Model
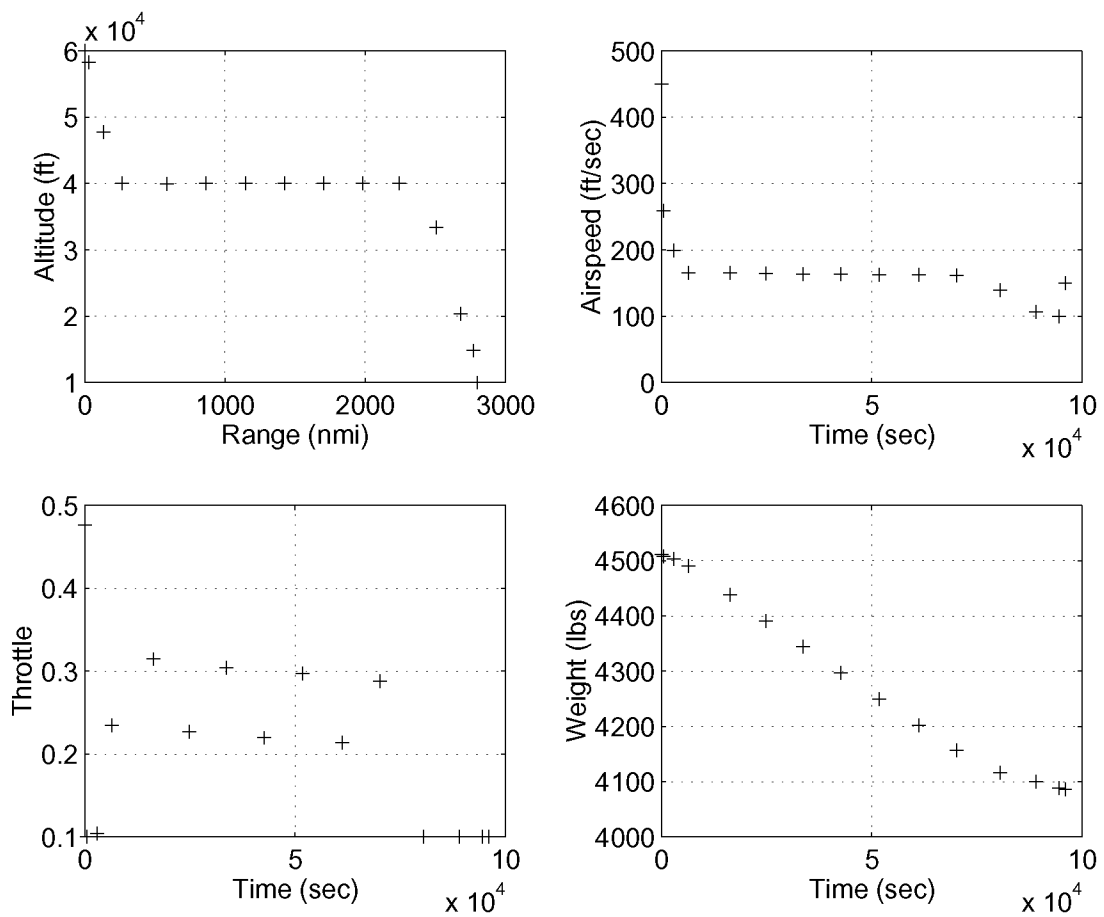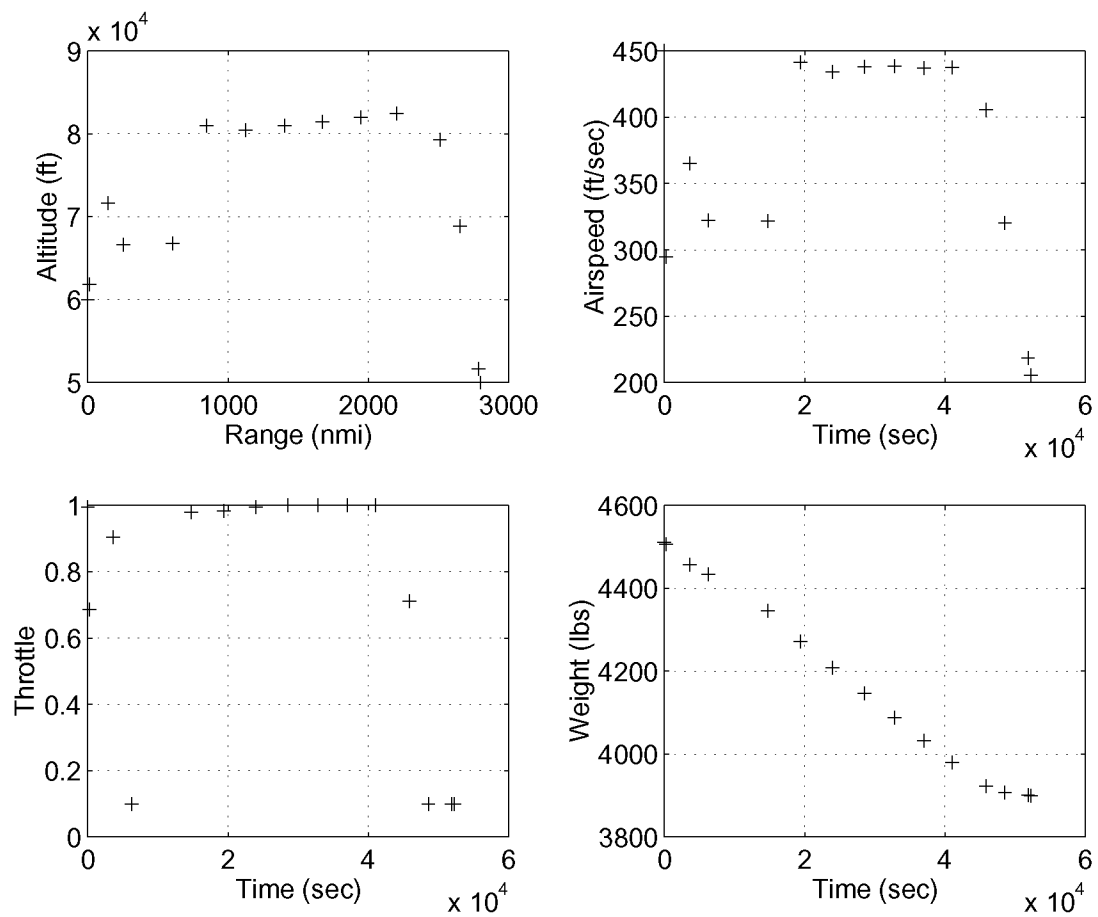
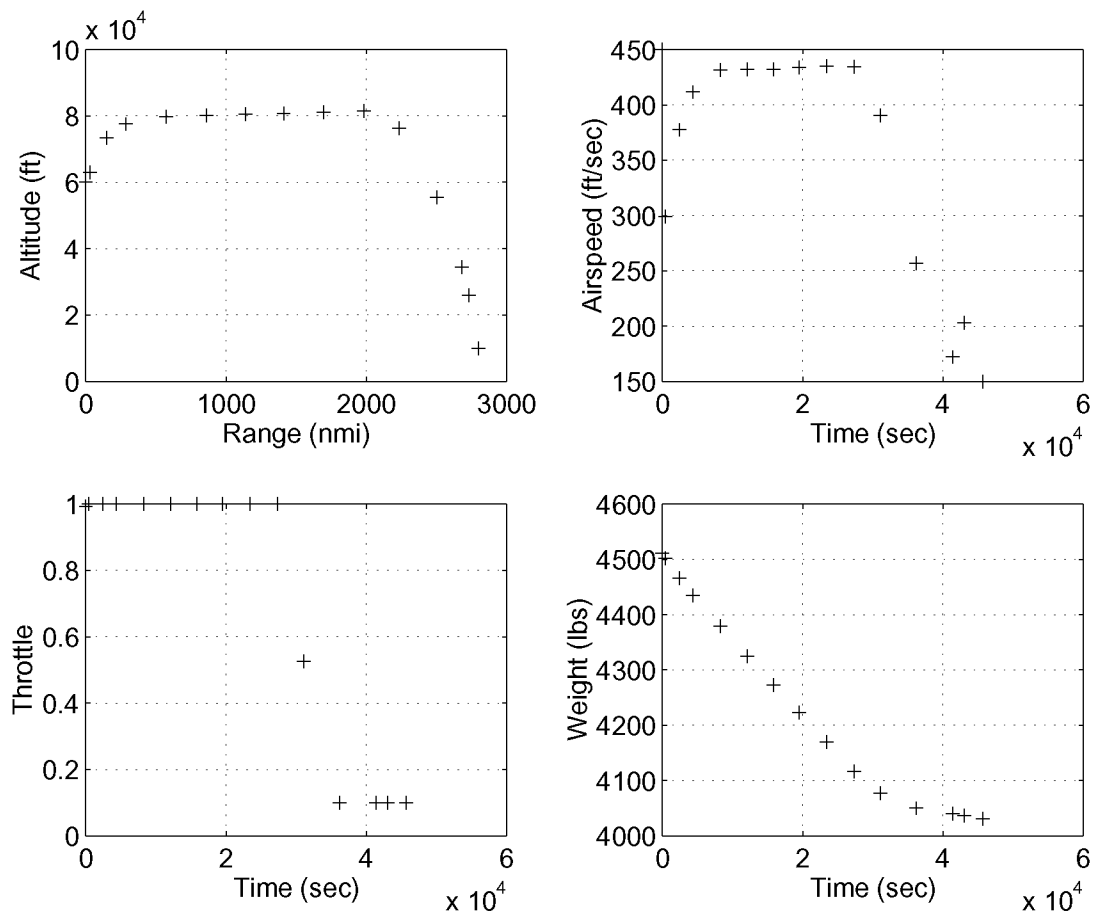Figure 5.15: 3-D, Starting Point B, $\mu = 0$, GSFC Wind Model

52
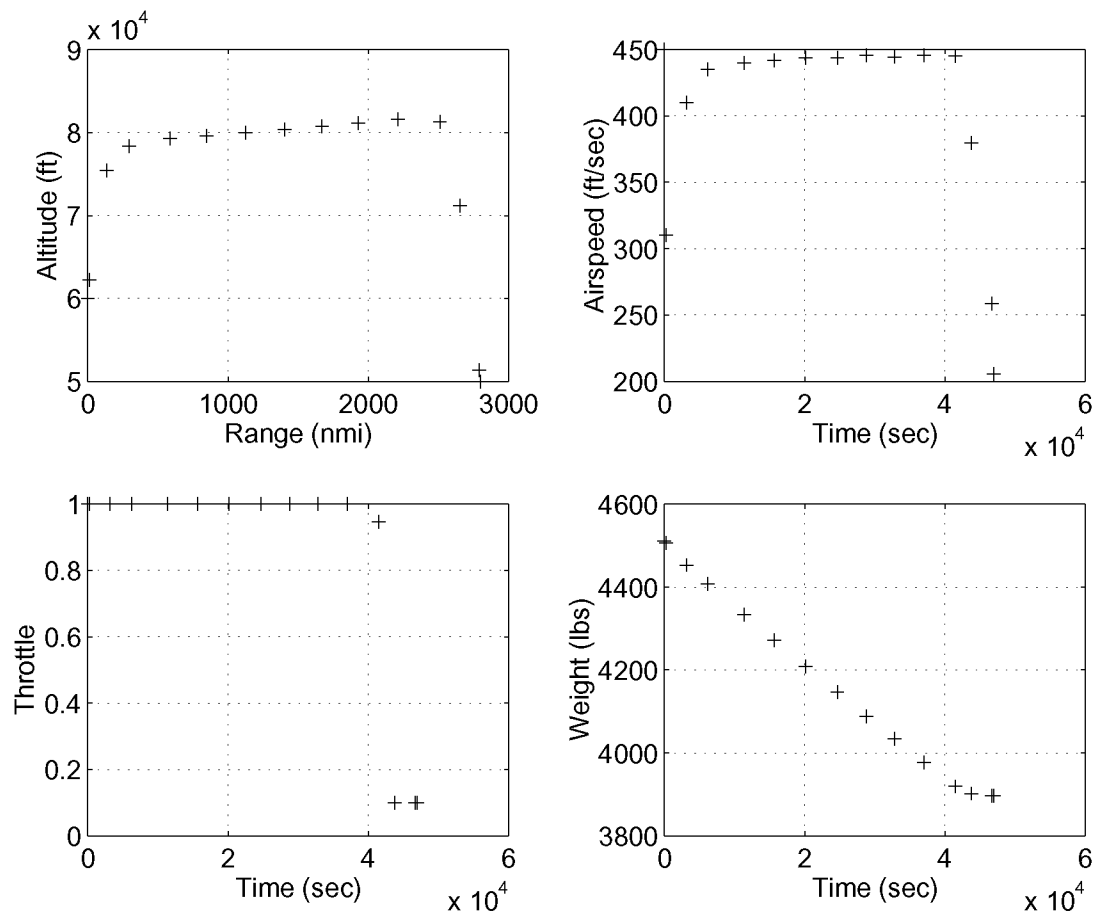
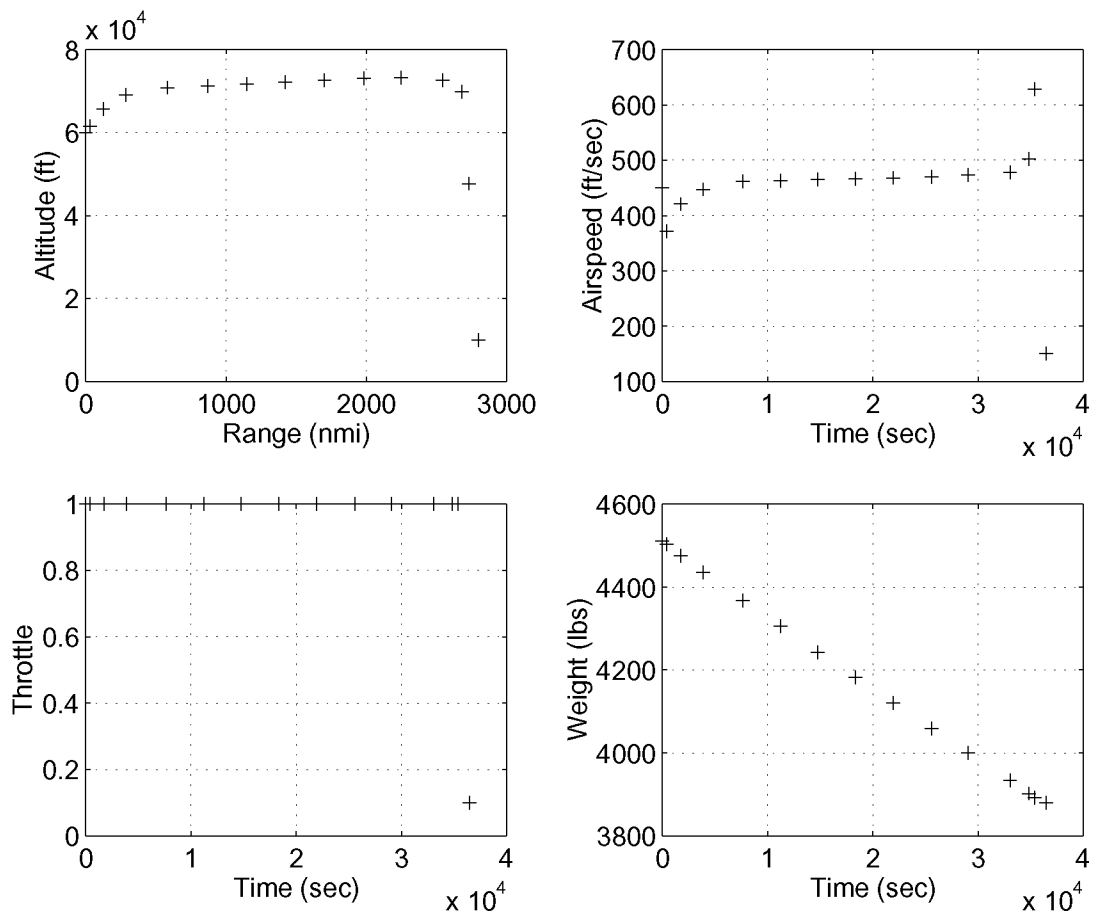Figure 5.16: 3-D, Starting Point B, $\mu = 3.048$ lb/sec, GSFC Wind Model

53

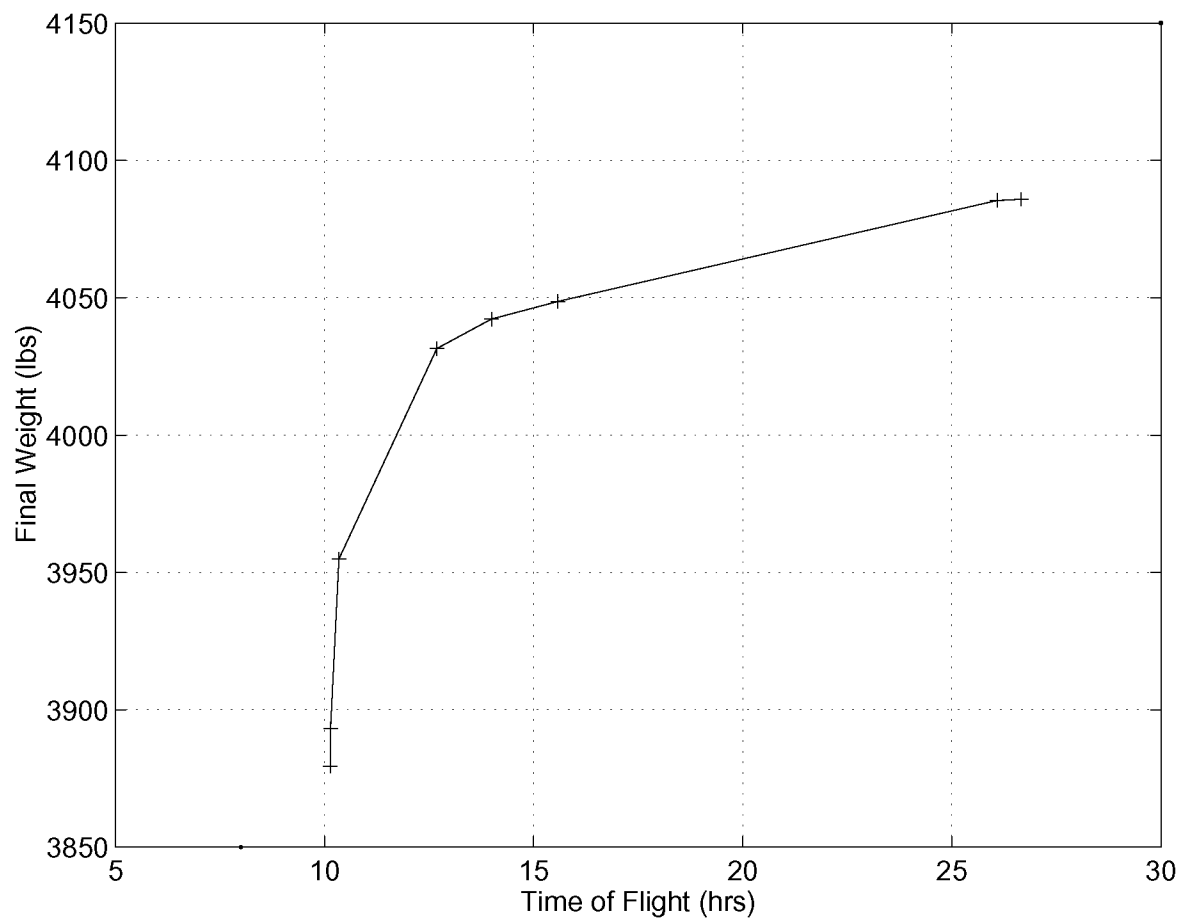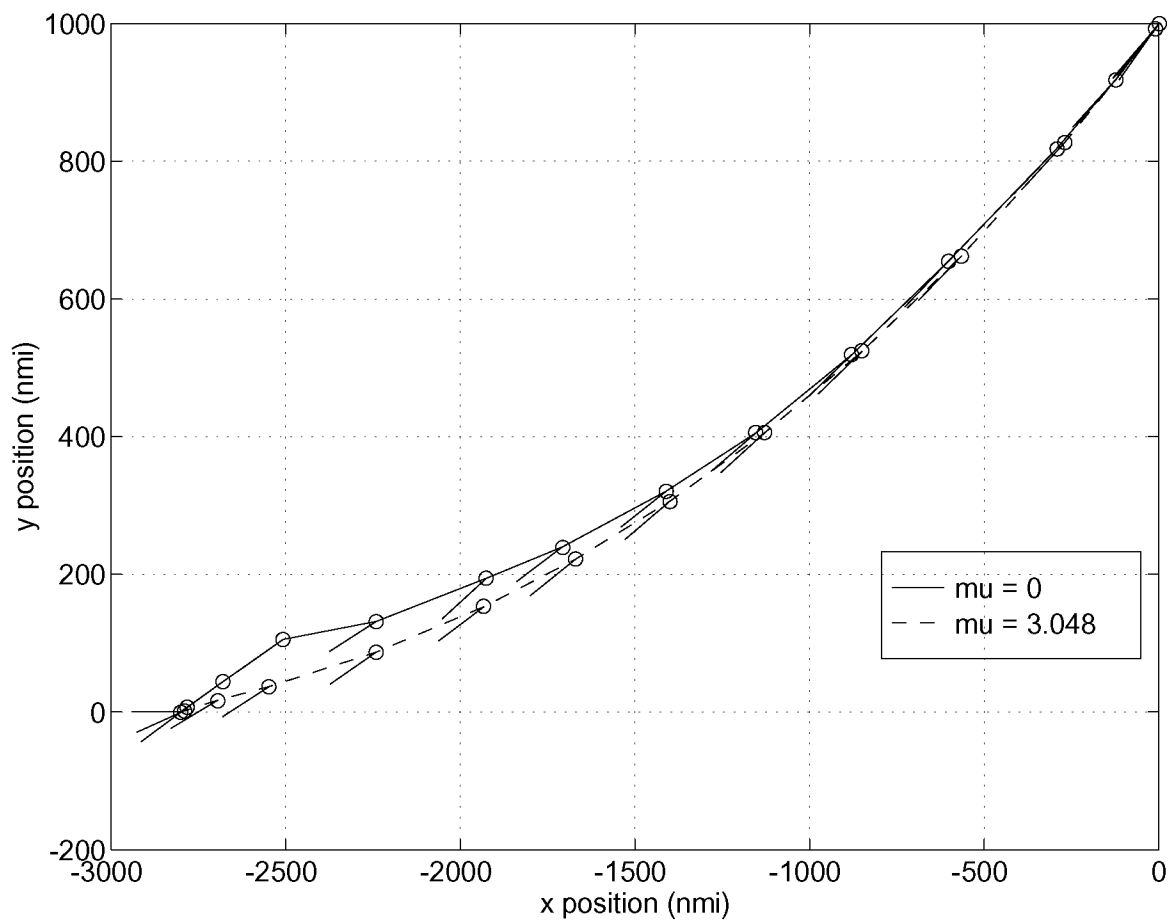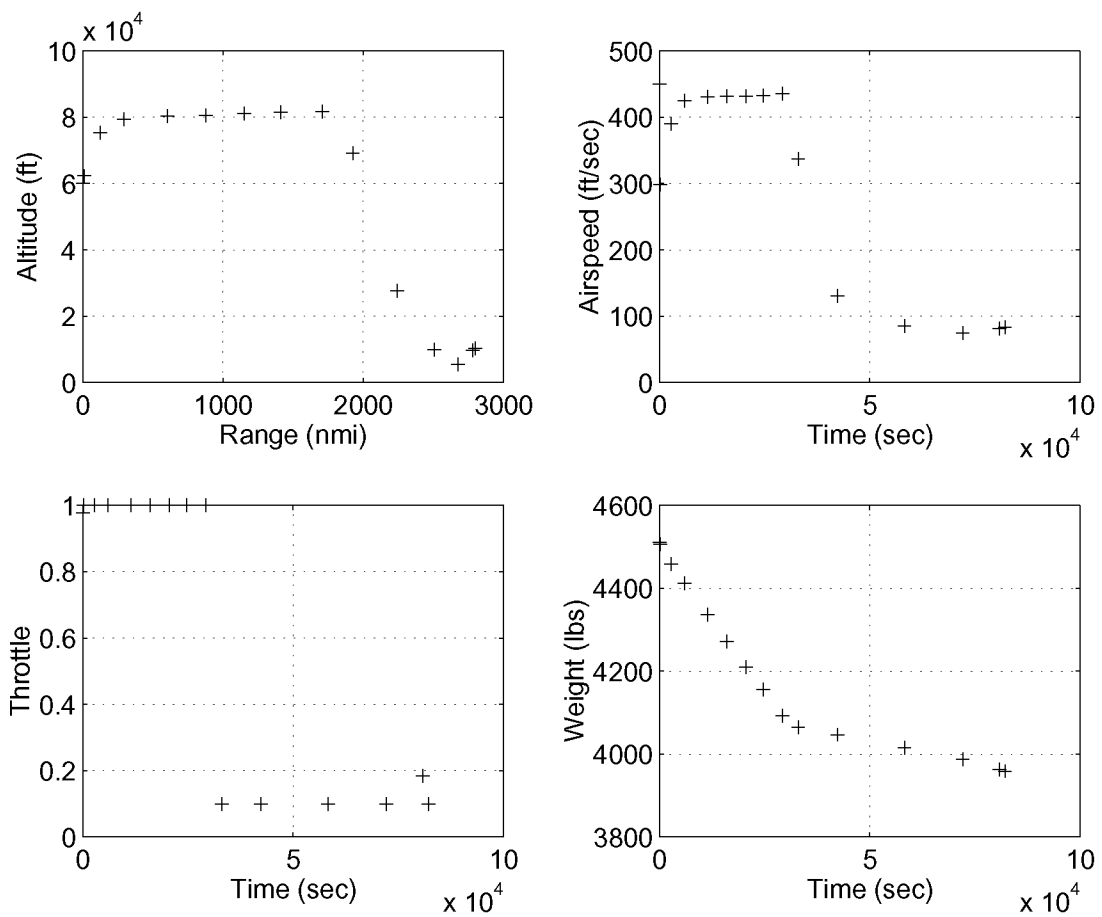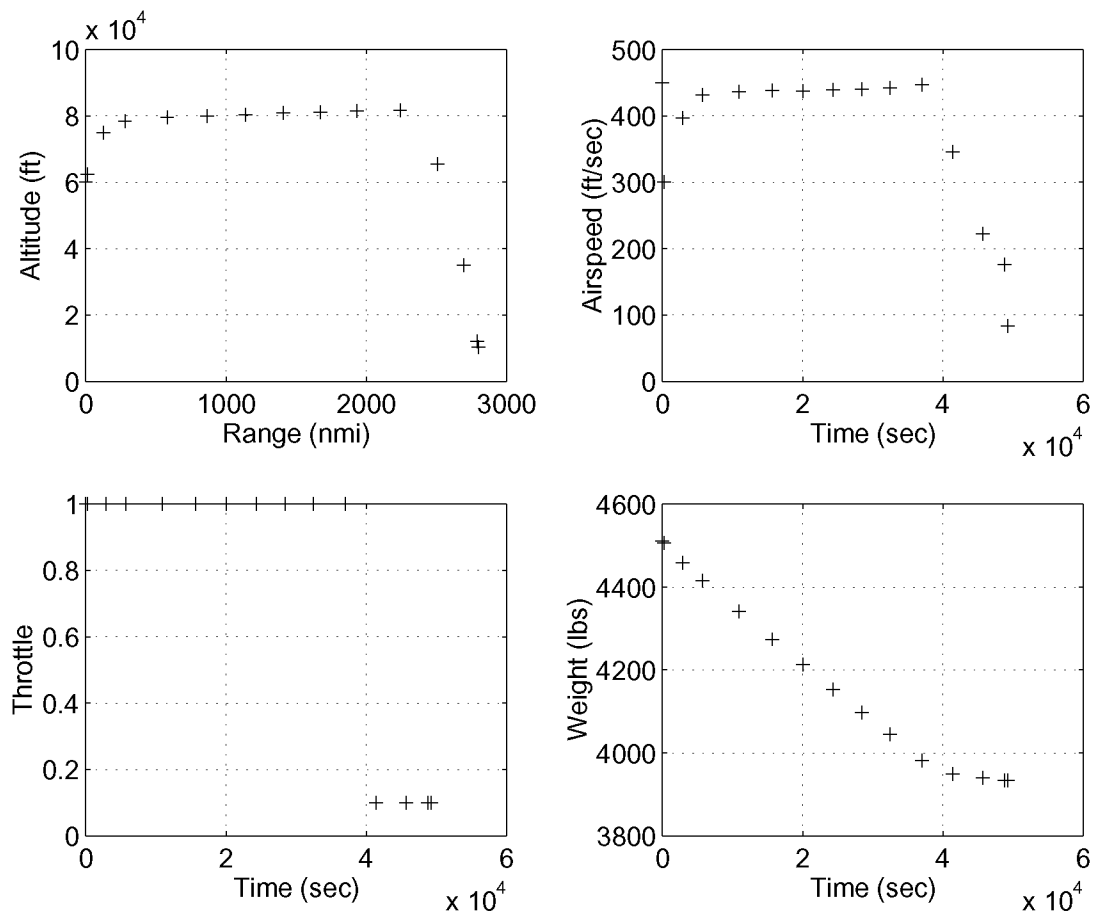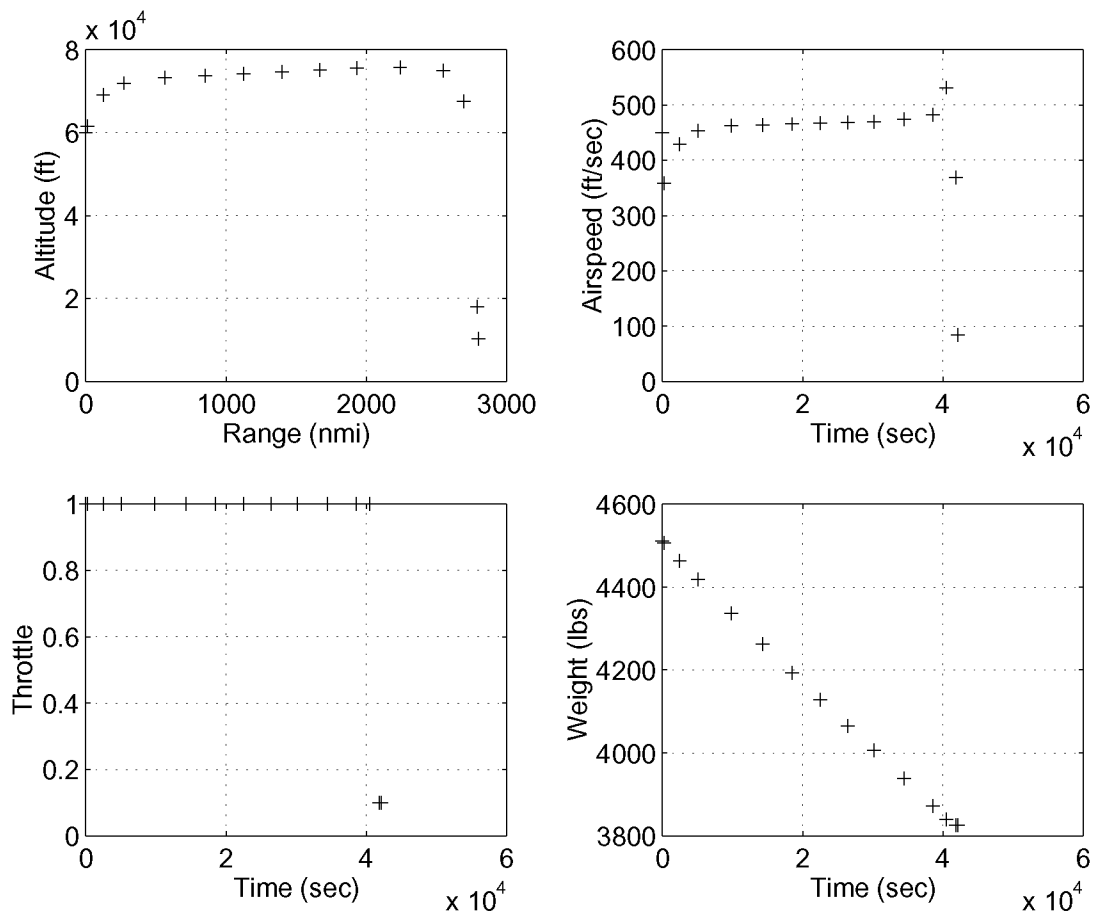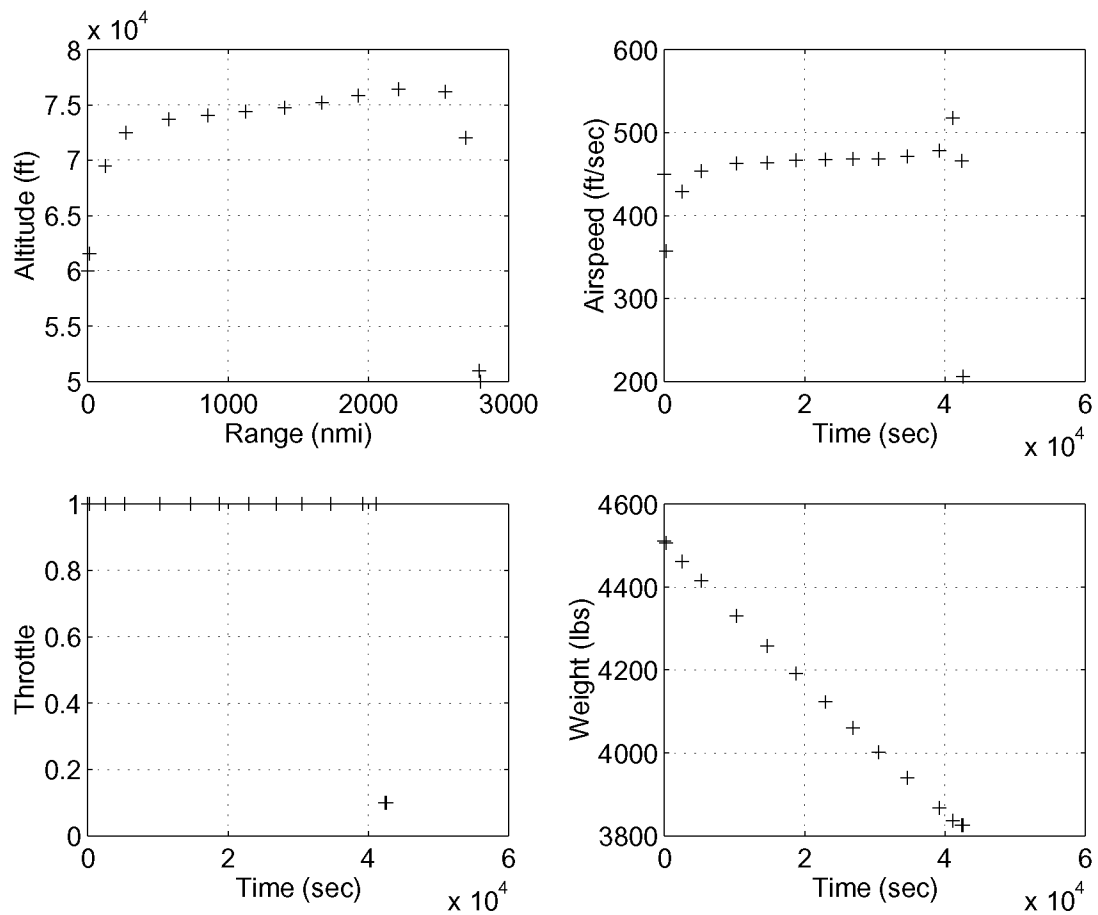Figure 5.17: 3-D, Starting Point B, $\mu = 3.048$ lb/sec, GSFC Wind Model
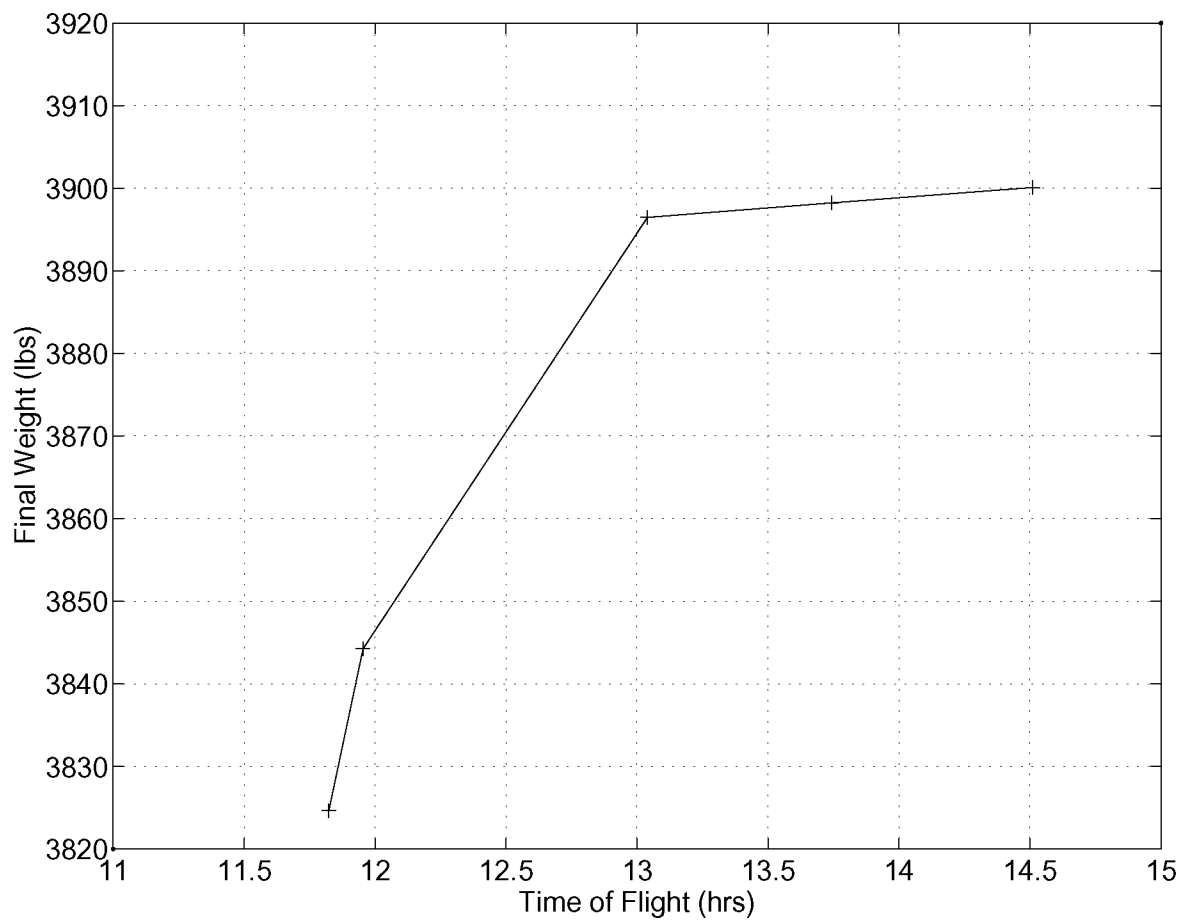
Figure 5.18: 3-D Family of Solutions, Starting Point B, GSFC Wind Model

Chapter 6

Continuous Optimal Control Formulation in the Vertical Plane

In this chapter a version of the flight optimization problem is studied in the context of optimal control. The intent is to find the structure of extremal paths from the optimality conditions with the objective of better understanding the numerical results detailed in Chapters 4 and 5. The results will not be used to calculate extremal paths; our numerical results are based on the NLP formulations described earlier.

6.1   Optimal Control Formulation of the Cruise Model

To get to the vertical plane cruise model we begin with the cruise model in Appendix A. First it is reduced in order by realizing that there is only one horizontal position coordinate now for range, x. Heading angle is always constant so χ is set equal to zero and the $\dot{\chi}$ equation is eliminated. The bank angle μ will also be set equal to zero since the aircraft will not be turning. Two states are equilibrated: $\dot{h} = 0$ implies that there is a small path angle or $\gamma = 0$ and $\dot{\gamma}$ means $L = W$. As mentioned in Section 2.2, velocity and altitude are combined into an energy state.

$$
\begin{aligned}
\dot{x} &= V + V_w \\
\dot{W}_f &= \frac{cP_a}{\eta} \\
\dot{E} &= \left(\frac{\xi \hat{P}_a}{W} - \frac{P_r}{W} \right)
\end{aligned}
\tag{6.1}
$$

To get a cruise model the energy model is simplified even more by setting $\dot{E} = 0$. This results in $P_a = P_r$. Now only two states remain:

$$
\begin{aligned}
\dot{x} &= V + V_w \\
\dot{W}_f &= \frac{cP_r}{\eta}
\end{aligned}
\tag{6.2}
$$

The controls are velocity, V, and altitude, h.

6.1.1 Derivation of the Breguet Range Equation

The Breguet range equation will now be derived for the case of no winds. In the cruise model the independent variable may be changed from time to range (x) so that there is only one state equation,

$$W_f' = \frac{dW_f}{dx} = \frac{cP_a}{\eta V}.$$

(6.3)

After integrating equation (6.3) and using a similar analysis to Anderson's [10] by assuming steady, level, unaccelerated flight and that η, L/D, and c are constant throughout the flight, the Breguet range equation is obtained.

$$R = \frac{\eta}{c}\frac{L}{D}\ln\frac{w_0}{w_1}$$

(6.4)

where w_0 is the initial weight of the aircraft and w_1 is the final weight. This shows that the airplane should instantaneously fly at $\left(\frac{L}{D}\right)_{max}$ in order to maximize the range. The corresponding velocity for minimum drag is as follows.

$$V_{md} = \sqrt{\frac{2W}{\rho S \left(C_L\right)_{md}}}$$

(6.5)

By looking at equation(6.5) it can be seen that as the weight of the aircraft decreases the minimum drag velocity will decrease. The velocity is also dependent on the air density so as the altitude increases, the density decreases and the velocity increases. Figure 6.1 shows these relationships graphically with curves of constant weight on a plot of altitude versus minimum drag velocity.

This analysis begins to explain why the vehicle tends to fly at the minimum drag velocity with $\mu = 0$ in the absence of winds as discussed earlier. Also the same case shows in Figure 4.1 that as the altitude increases the velocity increases which agrees with the previous analysis of equation(6.5).

When head winds and tail winds are added to the problem, basic flight mechanics [11] says that the airplane should fly at $u < 1$ in a tail wind and $u > 1$ in a head wind. This is consistent with what is seen in Section 4.2.

6.1.2 Hodograph

The term hodograph was coined by Hamilton in 1845 [12]. He was interested in the way the relative velocity vector (represented as a point in a plane) changed as two bodies moved under their mutual gravitational attraction. Hamilton observed that under Newtonian inverse-square gravitation the graph of the velocity vector is always a circle. In modern
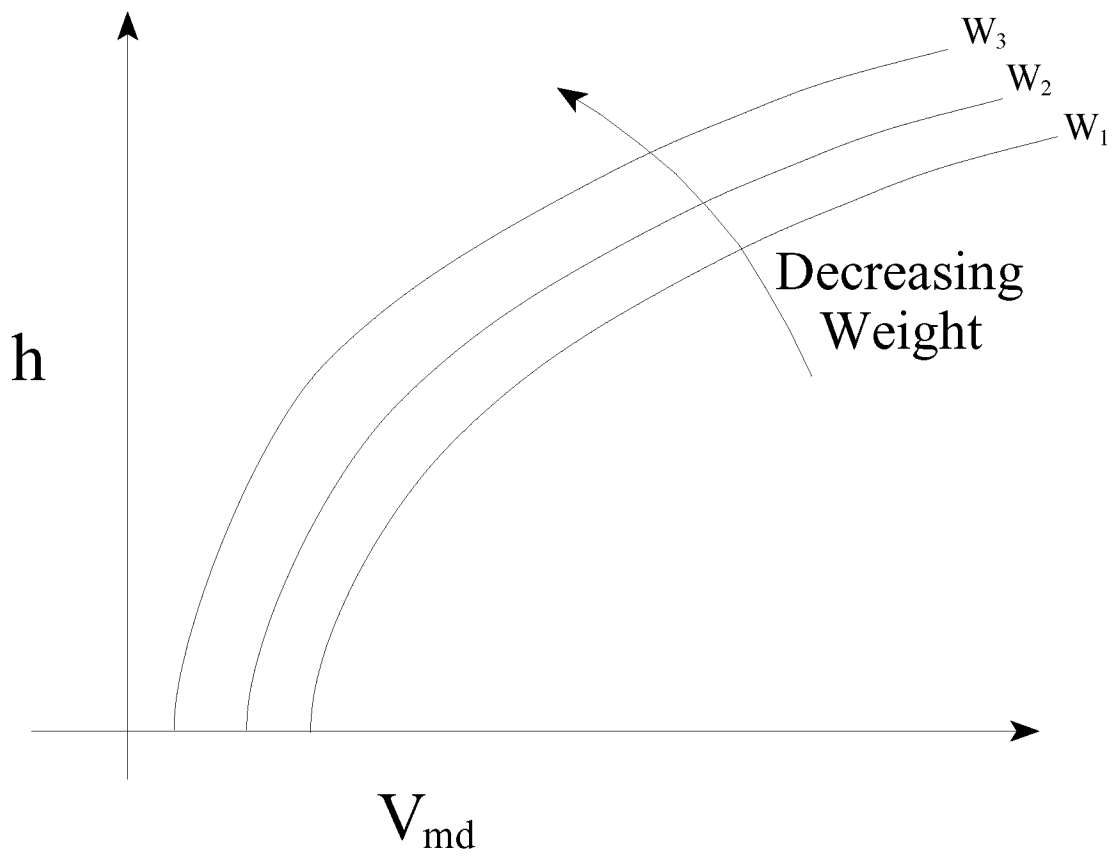
Figure 6.1: Minimum Drag Velocity Relationship to Altitude and Weight

control the term hodograph is used to describe the set of possible state-rates as the control is allowed to vary over admissible values. Using the ordinary differential equation representation,

$$\dot{z} = f(z, u),$$

we are interested in the set of points produced by the function f as u varies at fixed z. For the current application the state consists of two components namely x and W_f.

Getting a picture of the hodograph for the cruise model is a fairly simple task. There are two controls, velocity and altitude, so a two parameter family of points can be drawn. These are plotted as a family of curves; Each curve is plotted for a constant altitude while varying the vehicle airspeed, V, from a lower bound at the stall speed to an upper bound which causes the power required to exceed the maximum power available. Each curve is similar to the power required versus velocity curve since $\dot{W}_f$ is proportional to power required. The hodograph is pictured in Figure 6.2. The range rate and fuel rate values in this figure are nondimensional. The range rate is scaled by the velocity for minimum drag at standard sea level and standard weight, $\bar{V}_{md}$. The fuel rate is scaled by the standard weight divided by the time scale, W_s/T_{scl}, where $T_{scl} = \bar{V}_{md}/g$. It is drawn for the case where there are no winds. The curve which starts at the far left of the figure is the one corresponding to the lower bound due to the terrain, in this case $h = 0$ or sea level. As the altitude increases the curves move to the right and get shorter due to the velocity limits already mentioned. As shown in the figure there is an envelope created by these curves which appears to be linear in the middle portion between the range rates of approximately 1 and 2.

In order to show that the envelope is linear, Taylor and Mann's [13] method for determining envelopes of plane curves is used. We have a family of curves in the (ϕ, ψ) plane. Each curve is parameterized by a value of α. That is $F(\phi, \psi, \alpha) = 0$ at fixed α determines a curve in the plane. In the present case we have $\dot{x} = \phi$, $\dot{W}_f = \psi$ and $h = \alpha$.

$$\begin{aligned}
\dot{x} &= V \\
\dot{W}_f &= \frac{c}{\eta} P_r(V, h) \equiv f_1(V, h)
\end{aligned} \tag{6.6}$$

where $P_r(V, h)$ is the power required. A derivation of the power required equation is included in Appendix B. Rearranging equation (6.6) to be in the form $F(\phi, \psi, \alpha) = 0$ yields the following:

$$F(V, \dot{W}_f, h) = f_1(V, h) - \dot{W}_f = 0 \tag{6.7}$$

where V is used for $\dot{x}$. The condition on the envelope from Taylor and Mann [13] is

$$F_3(\phi, \psi, \alpha) = 0 \tag{6.8}$$

where $F_3 = \frac{\partial F}{\partial \alpha}$. When this condition is applied to equation (6.7), we find that $\frac{\partial f_1}{\partial h} = 0$. Solving this equation results in $V = V_{md}$. When this value of V is substituted back into

59
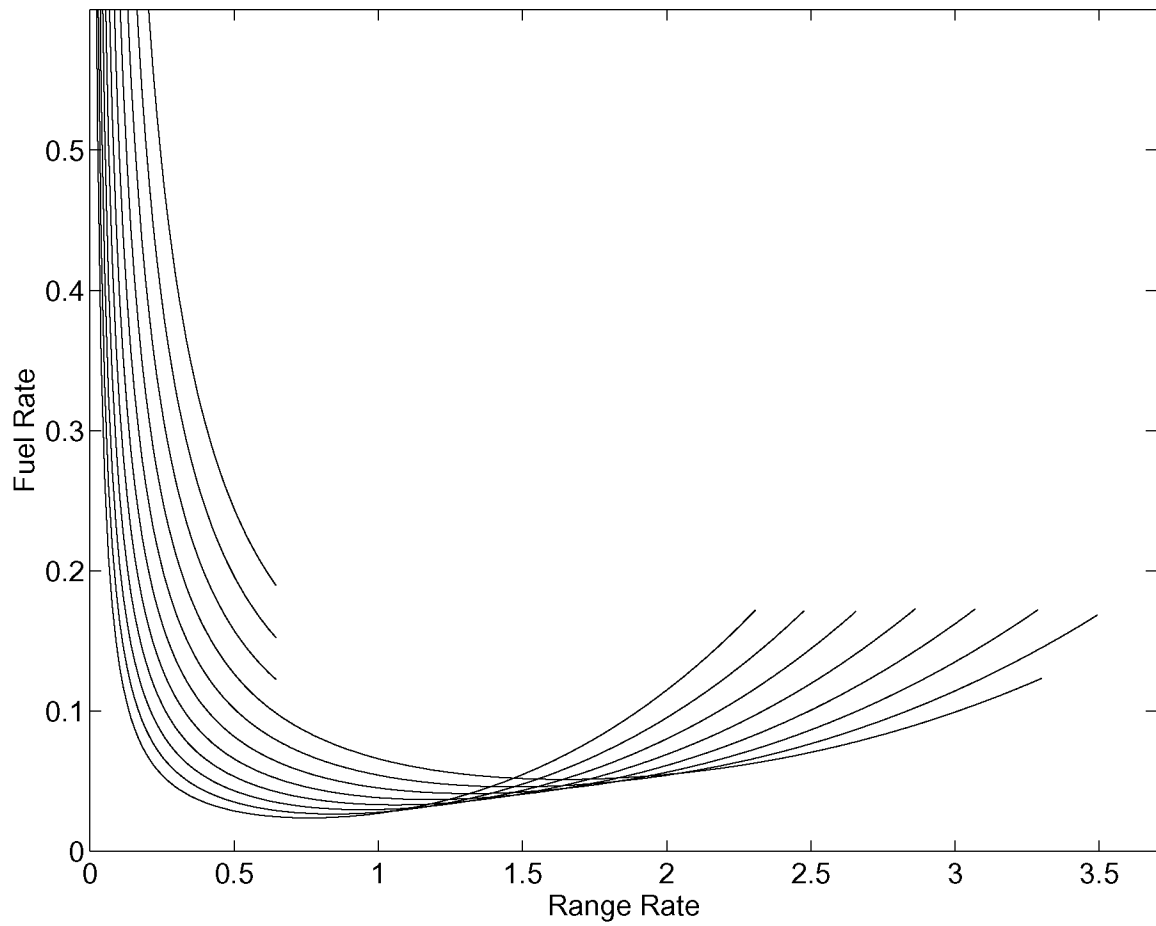
Figure 6.2: Cruise Model Hodograph

equation (6.6), the ratio of $\frac{\dot{W}_f}{\dot{x}}$ (the slope of the envelope) turns out to be a constant for a constant weight. This shows that the envelope is a straight line. The curved portions are only due to the limits on altitude. So, because $V = V_{md}$, the linear portion of the envelope corresponds to the airplane flying at maximum lift to drag.

6.1.3 Optimal Control Problem

There are lower and upper bounds on both controls. The lower bound on h will depend on the terrain being overflown. The lower bound on V is the stall speed of the airplane which is dependent on the altitude. There is an upper bound on the lift coefficient which has an effect on the maximum altitude at which the airplane can fly. The specific excess power must be greater than or equal to zero. This means that the maximum available power must be greater than or equal to the power required, $P_{a_{max}} \geq P_r$. The throttle setting, ξ, is multipled by the maximum power available and can be adjusted between 0 and 1 so that $\xi P_{a_{max}} = P_r$.

The following summarizes all of the limits placed on the controls.

$\beta_1 = (h - h_T) \geq 0$ (terrain limit)
$\beta_2 = (V - V_{stall}) \geq 0$ (stall velocity limit)
$\beta_3 = (C_{L_{max}} - C_L(V, h)) \geq 0$ (maximum lift coefficient limit)
$\beta_4 = P_{s_{max}(V,h)} \geq 0$ (specific excess power)

Using Bryson and Ho's [1] notation, the performance index can be a function of both the states at the final time, $z(t_f)$, and the final time itself, t_f. In this case it will be a Mayer type function and more specifically it will be a linear combination of the weight of fuel consumed at the final time and the final time itself.

$$\phi(X(t_f), t_f) = W_f(t_f) + \mu t_f \tag{6.9}$$

where μ is some positive constant. By increasing the value of μ the emphasis on minimizing time increases; when $\mu = 0$ only fuel consumed is being minimized. Initial values of x and W_f are specified while a final value is specified only for x. The final constraint on range can be represented as $\psi = x(t_f) - x_f = 0$. As in Bryson and Ho [1], a new scalar function, Φ, a linear combination of the performance index and the constraints, ψ, is defined as the following:

$$\Phi = \phi + \nu \psi \tag{6.10}$$

The variational Hamiltonian, H, is as follows:

$$H = \lambda_x \dot{x} + \lambda_w \dot{W}_f \tag{6.11}$$

61

where λ_x and λ_w are the co-states. To have an optimal solution the Hamiltonian must be minimized over the possible set of control values. If the constraints (β_i) are not active then the following conditions apply:

$$\frac{\partial H}{\partial V} = 0$$
$$\frac{\partial H}{\partial h} = 0$$

We shall examine the minimization of H from a geometric view based on the hodograph.

The costate vector λ (created by the costates λ_x and λ_w) can be plotted on the same $\dot{W}_f$ versus $\dot{x}$ plane as the hodograph. Since the Hamiltonian is a dot product of the costate vector and the state rate vector, lines of constant Hamiltonian are perpendicular to the costate vector as shown in Figure 6.3. The direction of increasing Hamiltonian is in the direction of the costate vector.

The optimality condition requires that we find a constant H line that separates the hodograph plane into a part that contains the achievable state-rates and a part that has no achievable state-rates. This line will be 'tangent' to the envelope of the hodograph in Figure 6.2.

The transversality conditions [1] include the requirement that $H = -\mu$. For the fuel optimal (only) case we have $\mu = 0$ and this means the constant H line must go through the origin.

Combining the tangency requirement and the $H = 0$ requirement we find that all points along the 'flat part' of the hodograph satisfy the optimality condition. This means that in cruise approximation, minimum fuel flight with no winds always occurs at the minimum drag velocity. The central part of our NLP solutions are nearly in equilibrium and display this feature.

For positive μ the separating H line must be below the origin ($\dot{W}_f < 0$ at $\dot{x} = 0$). This leads to a tangency point on the envelope of the hodograph which is also on the maximum altitude curve as is seen in Figure 6.4. When μ is large, the solution is at the upper bound of altitude. As μ is decreased from that value the constant H line moves closer to the origin and the solution point moves towards the linear portion of the envelope curve as shown in Figure 6.4.

Some insight into why certain behavior is seen in some of the numerical results was gained by this analysis. First of all, it was found that the airplane should fly at the minimum drag velocity in the absence of winds and with no emphasis on time. In the cases that were run with no winds and $\mu = 0$ the airplane did fly at or very close to this velocity.

Another important result of this analysis was finding that the envelope of the cruise model hodograph is linear and that all points along that line are extremal. When $\mu = 0$, there is no unique answer. The cruise model says to fly at the conditions for any point along that linear extremal on the hodograph. These points correspond to the points along a constant weight curve in Figure 6.1 which means the airplane can fly at any altitude as long as it flies at the minimum drag velocity.
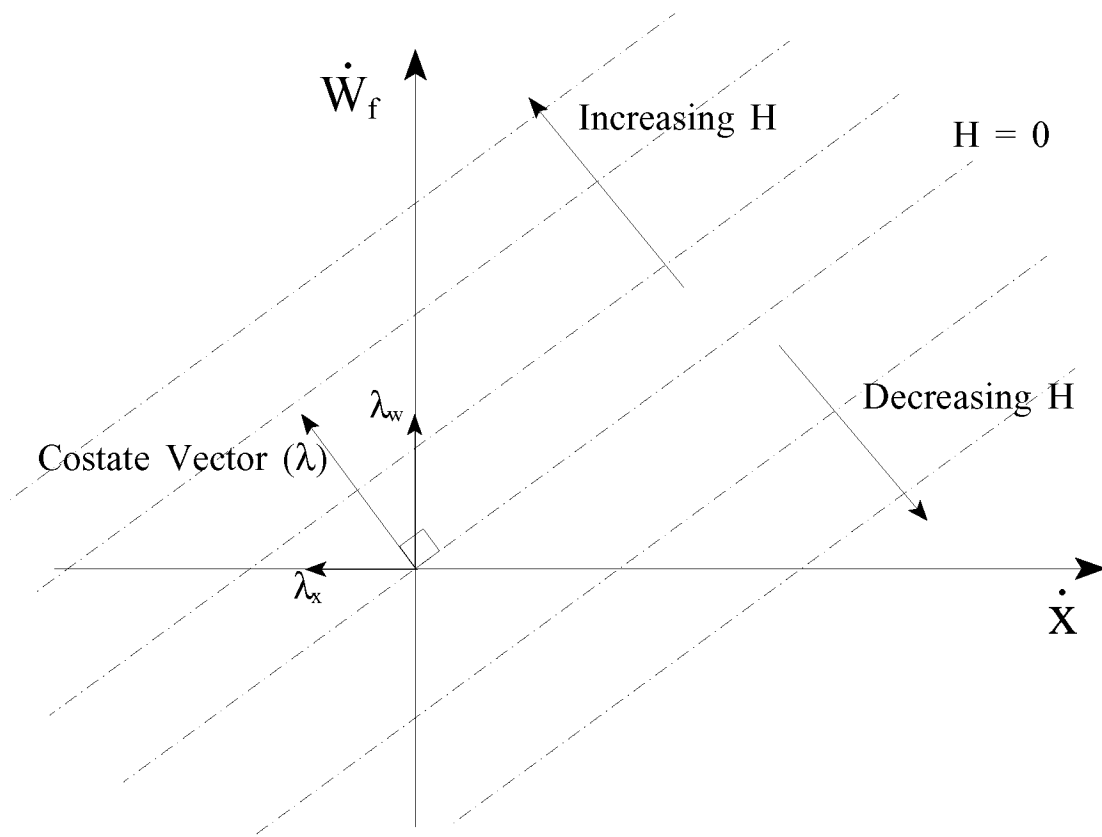
Figure 6.3: $\dot{W}_f$ versus $\dot{x}$: Lines of Constant Hamiltonian
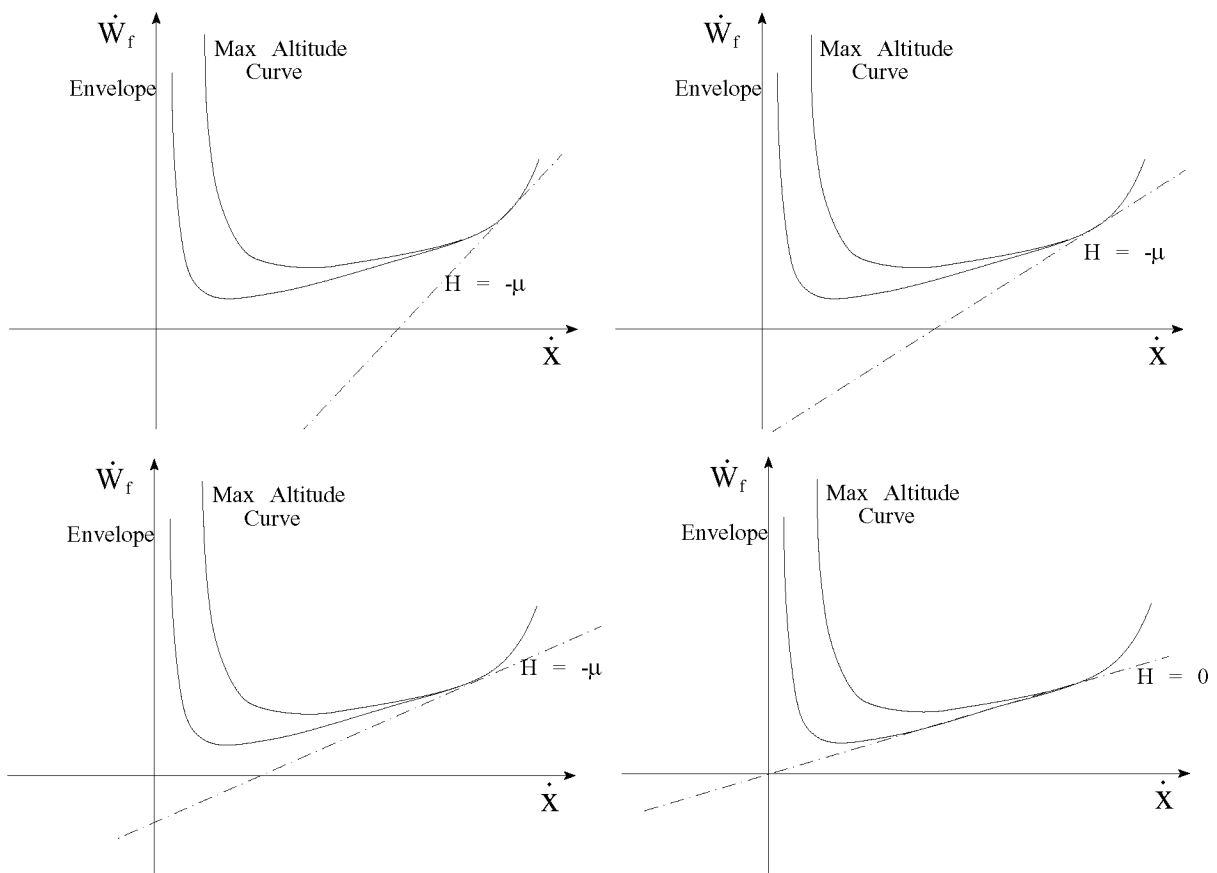
Figure 6.4: The Effect of Emphasis on Time on the Hamiltonian and Hodograph

Chapter 7

Summary and Conclusions

An energy model was developed for flight in a horizontal wind field. A Non-Linear Programming problem was formulated to optimize the flight path with a performance index based on a weighted sum of fuel-consumed and final time. Constraint equations were derived for kinematics, energy, and mass. The energy constraint included energy exchange due to turns made at the waypoints.

A prominent feature of the results in Section 5.2 can be interpreted as a three dimensional version of Zermelo's problem [1]; the winds act like currents and the vehicle flies in a path such that the winds can help it to its destination.

7.1 Throttle Oscillations

The oscillation in throttle setting seen in some of the results could possibly be due to the way the integral is approximated in the mass constraint equation. To approximate the integral a simple average was used:

$$\frac{\Delta t}{2}(\xi_r \ [\dot{W}_{f_r}]_{max} + \xi_l \ [\dot{W}_{f_l}]_{max}).$$

In the near cruise condition the maximum flow-rates are nearly identical so that the integral is essentially $\Delta t[\dot{W}_f]_{max} \cdot (\xi_r + \xi_l)/2$. Any change in the pair ξ_r, ξ_l that produces the same average will produce the same fuel flow-rate. This argument also applies to the power available.

As an alternative formulation, perhaps the left value of the throttle setting, ξ_l, should have been used for the whole calculation since the controls are assumed to be piecewise constant, not piecewise linear.

7.2 Effects of Energy Interchange

The effects of the energy interchange are more subtle. The total energy change between waypoints ($E_r - E_l$) is the sum of several terms: specific excess power term with no winds from first integral in equation (3.21), energy terms due to winds from last two integrals in equation (3.21), energy due to banked lift in the turn from equation (3.25), and energy due to maneuvering drag from equation (3.31). Typical ascending and near cruise condition waypoints were selected from the three dimensional problem with the analytic wind model. The waypoints selected from the ascending portion of the flight were 120.6 nmi apart from each other in the horizontal direction and were 11,040 ft apart in altitude. These waypoints had the following energy interchanges between them:

$E_r - E_l$ = 11,084.6 ft

$\int P_s \, dt$ = 11,023.7 ft

$\int P_s \, \mathcal{F} \, dt - \int \mathcal{F} \, dh$ = 60.96 ft

Banked lift term = 0.509 ft

Maneuvering drag term = -0.00561 ft

The turning terms were not significant (about 0.51% of total energy change between two waypoints) in climbing portion of the flight.

The waypoints selected from the near level portion of the flight were 328.2 nmi apart from each other in the horizontal direction and were 1,030 ft apart in altitude. These waypoints had the following energy interchanges between them:

$E_r - E_l$ = 6.57 ft

$\int P_s \, dt$ = -4.237 ft

$\int P_s \, \mathcal{F} \, dt - \int \mathcal{F} \, dh$ = -3.080 ft

Banked lift term = 5.391 ft

Maneuvering drag term = -0.0299 ft

The term due to the banked turn is significant (about 82% of total energy change between two waypoints) in this near level portion of the flight.

The change in total energy between the two waypoints is greater in the ascending portion of the flight due to a greater difference in altitude and velocity. There isn't much difference between the altitudes of the waypoints in the near level portion of the flight so the energy terms due to turning make up a greater percentage of the total energy change.

7.3 Software

It was seen that the computer run time generally decreased as emphasis on flight time (μ) increased. This was due to the solution point moving away from the linear portion of the hodograph so that there was a more definite and specific solution as was shown in Figure 6.4. As μ increased the vehicle went towards the maximum limits on throttle ($\xi = 1$) and altitude for a greater portion of the flight. With less emphasis on time the solution was on

the linear portion of the hodograph so any point along that line was a solution so it took more iterations to come to a specific one.

The results of this paper can be used in the flight planning of the Theseus vehicle by having the human operator choose from family of solutions depending on a desired landing time. A family of solutions such as the one in Figure 5.18 can be created in the time it takes to run about 4 to 5 cases of varying μ factors. This turns out to be only about 1 to 5 minutes, so the family can be found quickly and a flight plan selected while the airplane is flying.

Finally, the computer code developed for this paper can be used in general for flight planning of any vehicle of this class flying in a horizontal wind field. The code is modular and requires a subroutine for the specific aircraft engine model where the input is the current air velocity and altitude and the output is the maximum thrust power available and the maximum fuel flow rate. A subroutine for the winds is also necessary. The wind model is given an altitude and distance from the Pole and it returns a wind speed. Some specific data for the aircraft is also needed such as the parabolic drag data.

Bibliography

[1] Bryson, A.E. and Ho, Y.-C., *Applied Optimal Control*, Hemisphere Publishing Corporation, New York, 1975.

[2] Seywald, H. and Cliff, E.M., "Goddard Problem in the Presence of a Dynamic Pressure Limit", *Journal of Guidance, Control and Dynamics*, Volume 16, Number 4, pp. 776-781, July/August 1993.

[3] Brauer, G.L., Cornick, D,E., and Stevenson, R., *Capabilities and Applications of the Program to Simulate Optimized Trajectories (POST)*, NASA CR-2770, February 1977.

[4] Paris, S.W., Hargraves, C.R. and Martens, P.J., *Optimal Trajectories by Implicit Simulation (OTIS), Formulation Manual, WRDC-TR-90-3056, Volume I*, Wright Laboratories, WPAFB, OH, Decmber 1990

[5] Sorenson, J.A., Waters, M.H. and Patmore, L.C., *Computer Programs for Generation and Evaluation of Near-Optimum Vertical Flight Profiles*, NASA CR-3688, May 1983.

[6] Collins, B.P., Haines, A.L., and Wales C.J., *A Concept for a Fuel Efficient Flight Planning Aid for General Aviation*, NASA CR-3533, March 1982.

[7] Merritt, S.R., Cliff, E.M. and Kelley, H.J., "Energy-modelled Climb and Climb-dash — the Kaiser technique", *Automatica*, Volume 21, Number 3, pp. 319-321, May 1985.

[8] Gill, P.E., Murray, W. and Wright M.H., *Practical Optimization*, Academic Press, New York, 1981.

[9] Halfman, R.L., *Dynamics*, Addison-Wesley, Reading, 1962.

[10] Anderson, J.D., *Introduction to Flight, Third Edition*, McGraw-Hill, New York, 1989.

[11] Course material from the Aerospace Research Pilot's School, Edwards Air Force Base, anon.

[12] Hamilton, "A New Method of Expressing in Symbolical Language the Newtonian Law of Attraction", *Proceedings of the Royal Irish Academy*, Volume 3, pp. 344-353, 1847.

[13] Taylor, A.E. and Mann, W.R., *Advanced Calculus*, Wiley, New York, 1972.

[14] Etkin, B., *Dynamics of Atmospheric Flight*, Wiley, 1972.

[15] Meriam, J.L. and Kraige, L.G., *Engineering Mechanics*, Vol. 2, *Dynamics*, Wiley, 1992.

[16] Miele, A., *Flight Mechanics*, Vol I, Addison-Wesley, 1962.

Appendix A

Point-Mass Model

Our dynamic model can be simplified for the case of 'low' speed, 'short' range flight 'near' the surface of the Earth. Therefore an approximation of a flat, non-rotating Earth is made so the analysis begins with the hypothesis that a reference frame with its origin at a fixed point on the Earth's surface is an *inertial* reference frame (called the *Earth-Fixed Inertial Frame*). Newton's Second Law implies that the equation

$$\vec{F} = m\frac{d^2\,\vec{r}}{d\,t^2}\,|_I \tag{A.1}$$

describes the motion of the mass point at $\vec{r}$ when subjected to the net applied force $\vec{F}$ at the current mass, m. Our first task will be to relate the second derivative term to meaningful engineering quantities, such as speed and flight-path angle. We will also develop some useful kinematics.

A.1 Relative Motions

To carry out this analysis in an efficient manner we consider a general situation with two reference frames (*cf* Sec. 5.1 in [14], see Fig.A.1). It may be convenient to think that $\mathcal{F}_I$ is the *fixed* reference frame and that $\mathcal{F}_M$ is the *moving* reference frame. The translational motion of $\mathcal{F}_M$ with respect to $\mathcal{F}_I$ is given by the (time-varying) position vector $\vec{R}(t)$. The rotational motion of $\mathcal{F}_M$ with respect to $\mathcal{F}_I$ is given by the (time-varying) angular velocity vector $\vec{\omega}(t)$.

Following developments in ([15], pp 383–386) we write

$$\vec{r} = \vec{R} + \vec{\rho} \tag{A.2}$$

and find that:

$$\frac{d\,\vec{r}}{d\,t}\,|_I = \frac{d\,\vec{R}}{d\,t}\,|_I + \frac{d\,\vec{\rho}}{d\,t}\,|_M + \vec{\omega} \times \vec{\rho} \tag{A.3}$$
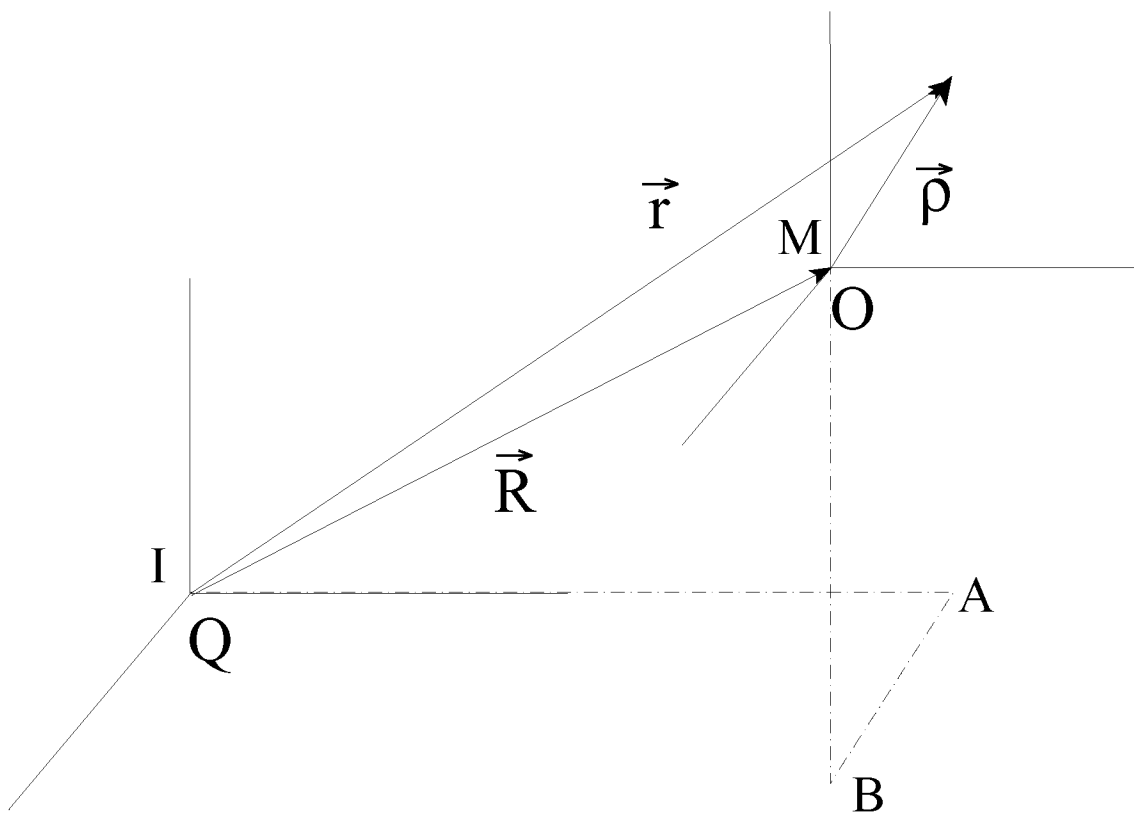
Figure A.1: Relative Motion

and that:

$$\frac{d^2\vec{r}}{dt^2}\big|_I = \frac{d^2\vec{R}}{dt^2}\big|_I + \dot{\vec{\omega}} \times \vec{\rho} + \vec{\omega} \times (\vec{\omega} \times \vec{\rho}) + 2\vec{\omega} \times \frac{d\vec{\rho}}{dt}\big|_M + \frac{d^2\vec{\rho}}{dt^2}\big|_M. \tag{A.4}$$

Note that with $\vec{R} \equiv 0$ (so that $\vec{r}(t) \equiv \vec{\rho}(t)$) equation (A.3) relates the *time-derivative* operation in one frame to that in a second frame. In the following we will be applying these principles to the flight motion problem. It is neccesary to clearly define the various reference frames; in particular we must describe the appropriate $\vec{\omega}$ relating the relative angular motion. We have already agreed that the *Earth-Fixed-Inertial* system provides our inertial frame and we will now introduce several other frames.

A.2 Reference Frames

The analysis in the section closely follows the development in [16]. A reference frame is arranged with origin Q at some fixed point on the surface of the Earth, and with x axis pointing North, y axis pointing East, and z axis pointing in the direction of gravity. This is the *Earth-fixed frame* as mentioned earlier and the symbol $\mathcal{F}_e$ is used to denote it.

The next reference frame – the *local horizontal frame*, $\mathcal{F}_h$ – will have its origin at the mass center of the flight vehicle. The position of the vehicle can be reckoned from the origin G of frame $\mathcal{F}_e$. Specifically, the location can be given in terms of a North/South position, x, an East/West position, y, and an altitude h above the Earth's surface. The coordinate axes are arranged so that they are parallel to the Earth-fixed axes.

There is no transformation needed from $\mathcal{F}_e$ to $\mathcal{F}_h$ since the two frames are aligned just as $\mathcal{F}_I$ and $\mathcal{F}_M$ appear to be aligned in Figure A.1.

We now recall that for the *wind-axes reference frame* - $\mathcal{F}_w$ - the origin is at the mass center of the flight vehicle, the x_w axis is aligned with the velocity of the vehicle (relative to the surrounding air mass), the z_w axis is in the symmetry plane of the vehicle, downward in the normal flight attitude, while the y_w axis completes the right-handed orthogonal set. The relative orientation of the frame $\mathcal{F}_w$ with respect to the local horizontal frame $\mathcal{F}_h$ is described by the velocity-yaw angle χ (heading angle), the velocity-pitch angle γ (flight-path angle), and the velocity-roll angle μ (bank angle). Composing these elementary rotations we find

$$L_{h \to w} = \begin{bmatrix} \cos\gamma\cos\chi & \cos\gamma\sin\chi & -\sin\gamma \\ \sin\mu\sin\gamma\cos\chi - \cos\mu\sin\chi & \sin\mu\sin\gamma\sin\chi + \cos\mu\cos\chi & \sin\mu\cos\gamma \\ \cos\mu\sin\gamma\cos\chi + \sin\mu\sin\chi & \cos\mu\sin\gamma\sin\chi - \sin\mu\cos\chi & \cos\mu\cos\gamma \end{bmatrix} \tag{A.5}$$

The relative angular velocity between $\mathcal{F}_h$ and $\mathcal{F}_w$ is due to changes in the angles χ, γ and μ. The usual analysis leads to:

$$\vec{\omega}_{w/h} = p_w \hat{i}_w + q_w \hat{j}_w + r_w \hat{k}_w , \tag{A.6}$$

where

$$\begin{bmatrix} p_w \\ q_w \\ r_w \end{bmatrix} \equiv \begin{bmatrix} 1 & 0 & -\sin\gamma \\ 0 & \cos\mu & \sin\mu\cos\gamma \\ 0 & -\sin\mu & \cos\mu\cos\gamma \end{bmatrix} \cdot \begin{bmatrix} \dot{\mu} \\ \dot{\gamma} \\ \dot{\chi} \end{bmatrix} \tag{A.7}$$

$\vec{\omega}_{h/e} = \vec{0}$, implying that $\vec{\omega}_{w/h} = \vec{\omega}_{w/e}$. The angular rate of $\mathcal{F}_w$ relative to $\mathcal{F}_e$ is the same as that of $\mathcal{F}_w$ relative to $\mathcal{F}_h$.

A.3 Kinematics

The position of the flight vehicle has been described in terms of x (positive to the North), y (positive to the East) and h (altitude). Clearly, the velocity will be related to the rate of change of these quantities. Using the point notation from Figure A.1 and letting the Earth-fixed frame be $\mathcal{F}_I$ and the horizontal frame be $\mathcal{F}_M$ in the figure the following is true:

$$\begin{aligned} \vec{V}_I &\equiv \frac{d\,\overrightarrow{(QO)}}{d\,t}\,\big|_e \\ &= \frac{d\,\overrightarrow{(QA)} + \overrightarrow{(AB)} + \overrightarrow{(BO)}}{d\,t}\,\big|_e \\ &= \frac{d\,x\,\hat{\imath}_h}{d\,t}\,\big|_e + \frac{d\,y\,\hat{\jmath}_h}{d\,t}\,\big|_e + \frac{d\,-h\,\hat{k}_h}{d\,t}\,\big|_e \\ &= \dot{x}\,\hat{\imath}_h + \dot{y}\,\hat{\jmath}_h - \dot{h}\hat{k}_h \end{aligned} \tag{A.8}$$

where $\vec{V}_I$ is the inertial velocity and is the vector sum of the airplane's velocity with respect to the surrounding air and wind velocity so that

$$\vec{V}_I = \vec{V} + \vec{V}_w. \tag{A.9}$$

In this case the winds are in the horizontal direction only so

$$\vec{V}_w = \vec{V}_{wx}\,\hat{\imath}_h + \vec{V}_{wy}\,\hat{\jmath}_h \tag{A.10}$$

$\vec{V}_{wx}$ and $\vec{V}_{wy}$ are the horizontal components of the wind velocity. Solving equation (A.9) for $\vec{V}$ and substituting in equations (A.8) and (A.10) yields the following equation:

$$\vec{V} = \dot{x}\,\hat{\imath}_h + \dot{y}\,\hat{\jmath}_h - \dot{h}\hat{k}_h - \vec{V}_{wx}\,\hat{\imath}_h - \vec{V}_{wy}\,\hat{\jmath}_h \tag{A.11}$$

We also have

$$\vec{V} = V\,\hat{\imath}_w = V(\cos\gamma\cos\chi\,\hat{\imath}_h + \cos\gamma\sin\chi\,\hat{\jmath}_h - \sin\gamma\,\hat{k}_h\,), \tag{A.12}$$

The two equations (A.11 and A.12) provide equivalent expressions for the vector $\vec{V}$. Equating components leads us to:

$$
\begin{aligned}
\dot{x} &= V \, \cos\gamma\cos\chi - \vec{V}_{wx} \\
\dot{y} &= V \, \cos\gamma\sin\chi - \vec{V}_{wy} \\
\dot{h} &= V\sin\gamma
\end{aligned}
\tag{A.13}
$$

The expression (A.13) provides the kinematic relation for our problem.

A.4 Inertial Acceleration

We now proceed with the main task of working out the expression for the acceleration term in (A.1).

From the definition of the inertial velocity in Equation (A.9) the inertial acceleration is now computed as:

$$
\frac{d\vec{V}_I}{dt}\Big|_e = \frac{d\vec{V}}{dt}\Big|_e + \frac{d\vec{V}_w}{dt}\Big|_e.
\tag{A.14}
$$

Before proceeding with a coordinate representation of the vector terms in (A.14), it is worth considering the question of which reference frame might be best for this purpose. While several choices are reasonable, the most common in the study of flight paths is the *wind-axes system*. One reason for this choice is the representation of the aerodynamic force.

Based on (A.14) the inertial acceleration will be composed of two terms. Since we opt for wind-axes, it is natural to compute the first of these as:

$$
\frac{d\vec{V}}{dt}\Big|_e = \frac{d\vec{V}}{dt}\Big|_w + \vec{\omega}_{w/e} \times \vec{V},
$$

and expanding the cross-product term we find

$$
\frac{d\vec{V}}{dt}\Big|_e = \dot{V}\hat{\imath}_w + V\left(r_w\hat{\jmath}_w - q_w\hat{k}_w\right).
\tag{A.15}
$$

The second (wind) term in (A.14) is found to be:

$$
\begin{aligned}
\frac{d\vec{V}_w}{dt}\Big|_e &= \frac{d\vec{V}_w}{dt}\Big|_h \\
&= \dot{\vec{V}}_{wx}\,\hat{\imath}_h + \dot{\vec{V}}_{wy}\,\hat{\jmath}_h
\end{aligned}
\tag{A.16}
$$

where $\dot{\vec{V}}_{wx}$ and $\dot{\vec{V}}_{wy}$ are the horizontal components of the wind acceleration. Transforming into the wind axes components,

$$
\begin{bmatrix}
\dot{W}_1 \\
\dot{W}_2 \\
\dot{W}_3
\end{bmatrix}
= L_{h\rightarrow w} \cdot
\begin{bmatrix}
\dot{\vec{V}}_{wx} \\
\dot{\vec{V}}_{wy} \\
0
\end{bmatrix}
\tag{A.17}
$$

When the vector representation is transformed into the wind axis system, there can be a third component of the wind acceleration in this system if the airplane is banking or pitching.

A.5 Force Representation

We commonly decompose the net force acting on the flight vehicle into *aerodynamic, propulsive* and *gravitational* contributions.

$$\vec{F} = \vec{A} + \vec{T} + \vec{W} \tag{A.18}$$

A.5.1 Aerodynamic Force

Symmetric flight is being assumed which means no side slip, $\beta = 0$, and no side force, $Q = 0$. The components of the aerodynamic force in the wind-axes systems are then denoted by drag and lift only; that is

$$\vec{A} = -(D\hat{\imath}_w + L\hat{k}_w). \tag{A.19}$$

The $D(\cdot)$ and $L(\cdot)$ functions are specific to the vehicle whose flight performance we wish to model.

A.5.2 Propulsive Force

In this case the thrust direction is always assumed to be in the aircraft velocity direction. Specifically, we find

$$\vec{T} = T\,\hat{\imath}_w \tag{A.20}$$

A.5.3 Gravitational Force

The gravitational force is easily represented in the $\mathcal{F}_h$ frame as $\vec{W} = mg(h)\hat{k}_h$. In this model acceleration due to gravity, g, is assumed to be constant at all altitudes. The components in the $\mathcal{F}_w$ frame can be found from the third column of the transformation matrix (A.5) which leads to

$$\vec{W} = mg\left(-\sin\gamma\,\hat{\imath}_w + \sin\mu\cos\gamma\,\hat{\jmath}_w + \cos\mu\cos\gamma\,\hat{k}_w\right). \tag{A.21}$$

A.6 Assembling the Pieces

Our objective is a dynamic model (in this case a system of ordinary differential equations), that will describe the time evolution of the position/velocity of the vehicle. We have chosen to parameterize the position in terms of $(x,\ y,\ h)$ and the velocity in terms of $(V,\ \gamma,\ \chi)$. The differential equations describing the evolution of $(x,\ y,\ h)$ have been given explicitly in (A.13). The model for the evolution of $(V,\ \gamma,\ \chi)$ is more intricate.

Our basic equation is (A.1). The description of the acceleration term has been done in Section (5), while the force terms were analyzed in Section (6). We have elected a *wind-axes* resolution of the vectors. To describe the process for extracting $\dot{V}$, $\dot{\gamma}$, and $\dot{\chi}$, it is helpful to write our version of (A.1) as:

$$m\left(\dot{V}\,\hat{\imath}_w \;+\; V\left(r_w\hat{\jmath}_w \;-\; q_w\hat{k}_w\right)\right) = \vec{A} + \vec{T} + \vec{W} - m\left(\dot{W}_1\,\hat{\imath}_w \;+\; \dot{W}_2\,\hat{\jmath}_w \;+\; \dot{W}_3\,\hat{k}_w\right). \quad (A.22)$$

The wind-axes representations of the various terms on the right-side of (A.22) are given in the previous sections. Each term is computable from the current values of

$$(x,\; y,\; h,\; V,\; \gamma,\; \chi\,, m) \quad \text{and} \quad (\mu).$$

The former seven variables are called *state variables* - these are the variables whose evolution is governed by the differential equations. The latter variable, along with throttle-setting are called *control variables* - these are viewed as selectable by the pilot. The pilot (or auto-pilot) effects the motions of the vehicle through the choice of the (time-varying) controls.

The $\hat{\imath}_w$ component of (A.22) may be solved directly to obtain $\dot{V}$. The $\hat{\jmath}_w$ component yields r_w, while the $\hat{k}_w$ component yields q_w. With these known, the bottom two rows of the matrix equation (A.7) can be solved for $\dot{\gamma}$ and $\dot{\chi}$. The seventh state-variable is the mass of the vehicle - its rate of decrease is the fuel mass-flow-rate which must be described as part of the propulsive model.

The last two rows of (A.7) can be manipulated to produce:

$$\dot{\gamma} \;=\; \cos\mu\; q_w \;-\; \sin\mu\; r_w$$
$$\cos\gamma\,\dot{\chi} \;=\; \sin\mu\; q_w + \cos\mu\; r_w$$

Combining this with (A.22) leads to our model:

$$\dot{V} \;=\; (T - D - mg\sin\gamma)\,/m - W_1$$
$$\dot{\gamma} \;=\; \left[\frac{L}{m}\cos\mu - g\cos\gamma + \dot{W}_3\cos\mu + \dot{W}_2\sin\mu\right]/V \qquad (A.23)$$
$$\dot{\chi} \;=\; \left[\frac{L}{m}\sin\mu - \dot{W}_2\cos\mu + \dot{W}_3\sin\mu\right]/(V\cos\gamma)$$

The seventh state can be written as the rate of fuel consumed since the weight of fuel varies in the same way the weight of the entire aircraft varies. This seventh state is

$$\dot{W}_f = \frac{cP_a}{\eta} \qquad (A.24)$$

where W_f is the weight of fuel consumed, c is the specific fuel consumption, P_a is the power available, and η is the propeller efficiency.

Equations (A.13), (A.23), and (A.24) make up the point-mass model for symmetric flight over in flat non-rotating Earth in a horizontal wind field.

Appendix B

Calculation of Power Required

A procedure similar to ARPS [11] is followed to determine the PIW-VIW curve for the aircraft. A PIW-VIW curve is a nondimensional power versus velocity curve which is good for a certain aircraft configuration at any weight and altitude. Assuming a parabolic drag polar as in equation (3.27) and that $L = W$,

$$\frac{D}{W} = \frac{C_D}{C_L} = \frac{C_{D_o} + k\ C_L{}^2}{C_L} \tag{B.1}$$

After substituting $C_L = \frac{W/S}{\bar{q}}$ into equation (B.1) where $\bar{q}$ is the dynamic pressure we get:

$$\frac{D}{W} = \frac{C_{D_o}}{W/S}\ \bar{q} + \frac{k\ W/S}{\bar{q}} \tag{B.2}$$

Using the lift coefficient for minimum drag, $C_{Lmd} = \sqrt{C_{D_o}/k}$, the velocity for minimum drag is found to be

$$V_{md} = \sqrt{\frac{2(W/S)}{\rho_o\sqrt{C_{Do}/k}}}\ \frac{1}{\sqrt{\sigma}} = \frac{V_{emd}}{\sqrt{\sigma}} \tag{B.3}$$

where the e subscript in V_{emd} is for equivalent velocity so that $V_e = V\sqrt{\sigma}$ and $\sigma = \frac{\rho}{\rho_o}$. After substituting $\bar{q} = \frac{1}{2}\rho_o V_e{}^2$ and doing some algebra using V_{emd} in equation (B.2) the following expressions for the drag to weight ratio are obtained:

$$\begin{aligned} \frac{D}{W} &= \sqrt{C_{D_o}\ K}\left[u^2 + \frac{1}{u^2}\right] \\ &= \frac{[(L/D)_{max}]^{-1}}{2}\left[u^2 + \frac{1}{u^2}\right] \end{aligned} \tag{B.4}$$

where $u \equiv V/V_{md}$.

The power required to overcome the drag force is $P_r = D \cdot V$. Now the $\frac{D}{W}$ expression from equation (B.4) is substituted into P_r and both sides are multiplied by $\sqrt{\sigma}$ to get the following expression which is good for any altitude.

$$P_r\sqrt{\sigma} = \frac{[(L/D)_{max}]^{-1}}{2} (W \ V_{emd}) \left[u^3 + \frac{1}{u}\right] \tag{B.5}$$

The equivalent velocity for minimum drag still depends on weight so a distinction is made between weights. W_t will be the "test" or actual weight and W_s will be a standard weight (say the full weight of the aircraft). In all equations until now W has been the test weight. A new velocity parameter, independent of weight, is now introduced.

$$\bar{V} = \sqrt[4]{\frac{k}{C_{Do}}}\sqrt{\frac{2(W_s/S)}{\rho_o}} \tag{B.6}$$

$\bar{V}$ is the air speed for minimum drag at the standard weight and at standard sea level density. We have $V_{emd} = \bar{V}\sqrt{\frac{W_t}{W_s}}$. $\bar{V}$ is substituted into equation (B.5) and both sides are divided by $(W_t/W_s)^{3/2}$ and the scaling power, $W_s\bar{V}$ to get a nondimensional expression for all weights and altitudes.

$$\frac{\frac{P_r\sqrt{\sigma}}{(W_t/W_s)^{3/2}}}{(W_s \ \bar{V})} = \frac{[(L/D)_{max}]^{-1}}{2} \left[u^3 + \frac{1}{u}\right] \tag{B.7}$$

The parameters PIW and VIW are now defined nondimensionally as:

$$PIW \equiv \frac{\frac{P_r\sqrt{\sigma}}{(W_t/W_s)^{3/2}}}{(W_s \ \bar{V})}$$

$$VIW \equiv u = \frac{\left(V/\bar{V}\right) \ \sqrt{\sigma}}{\sqrt{W_t/W_s}}$$

Note that PIW only depends on VIW. The only data needed about the aircraft in order to draw its PIW-VIW curve, assuming a parabolic drag polar, is $(L/D)_{max}$ as shown in the following equation obtained by substituting the definitions of PIW and VIW into equation (B.7).

$$PIW = \frac{[(L/D)_{max}]^{-1}}{2} \left[VIW^3 + \frac{1}{VIW}\right] \tag{B.8}$$

A value for VIW can be found by knowing the following: $V/\bar{V}$, σ, and W_t/W_s. PIW can be calculated from VIW as in equation (B.8). Finally, the power required is obtained nondimensionally using values already mentioned from the following equation:

$$\frac{P_r}{(W_s \ \bar{V})} = \frac{PIW \ (W_t/W_s)^{3/2}}{\sqrt{\sigma}}$$

Appendix C

Aircraft Data

C.1   Aircraft Dimensions

maximum gross weight = 5511 lb
empty weight   = 3825 lb
wing area (S) = 678 ft^2
aspect ratio (AR) = 28

C.2   Flight Characteristics

The vehicle is to operate at high altitudes (60,000 - 80,000 feet) and low dynamic pressure, Q, (a few pounds per square ft) so it has been designed with a low wing loading, $C_L\, Q = W/S$. Since the Q is low, W/S has to be low. A parabolic drag polar, $C_D = C_{D_o} + k\, C_L^2$ is used where

e = 0.96
C_{D_o} = 0.0153
k = $(\pi A R e)^{-1}$ = 0.01184

C.3   Engine Model

The aircraft has two engines at 80 hp each.

Specific Fuel Consumption (c) = 0.45 lb/hr/HP
Propeller Efficiency   = 83%

The power available is constant up to 65,000 ft and will decrease linearly to 60% at 82,000 ft.

Vita

Michael A. Feldman

The author was born in Baltimore, Maryland on November first, nineteen hundred seventy two. He received a Bachelor of Science degree in Aerospace Engineering from Case Western Reserve University in May of 1994. This work is part of the requirement for a Master of Science degree in Aerospace Engineering at the Virginia Polytechnic Institute and State University.